INSTITUTO SUPERIOR DE ENGENHARIA DO PORTO
MESTRADO EM ENGENHARIA MECÂNICA




Fracture Characterisation of bonded joints between cortical bone tissue and bone cement

MARTA LUÍSA SOUSA BARBOSA
dezembro de 2021

POLITÉCNICO
DO PORTO

Instituto Superior de Engenharia do Porto

FRACTURE CHARACTERISATION OF BONDED JOINTS BETWEEN CORTICAL BONE TISSUE AND BONE CEMENT

Marta Luísa Sousa Barbosa

2021

ISEP – School of Engineering, Polytechnic of Porto
Mechanical Engineering Department

POLITÉCNICO DO PORTO

Instituto Superior de Engenharia do Porto

FRACTURE CHARACTERISATION OF BONDED JOINTS BETWEEN CORTICAL BONE TISSUE AND BONE CEMENT

Marta Luísa Sousa Barbosa
1160374

Dissertation presented to ISEP – School of Engineering, Polytechnic of Porto, to fulfil the requirements necessary to obtain a master's degree in Mechanical Engineering, carried out under the guidance of Doctor Francisco José Gomes da Silva, associate professor with habilitation at ISEP – School of Engineering, Polytechnic of Porto, and Doctor Marcelo Francisco de Sousa Ferreira de Moura, associate professor with habilitation at FEUP – Faculty of Engineering, University of Porto.

2021
ISEP – School of Engineering, Polytechnic of Porto
Mechanical Engineering Department

POLITÉCNICO
DO PORTO

"SATISFACTION LIES IN THE EFFORT, NOT IN THE ATTAINMENT, FULL EFFORT IS FULL VICTORY."

Mahatma Gandhi

JURY

President
Isabel Cristina Silva Barros Rodrigues Mendes Pinto, PhD
Adjunct Professor, ISEP – School of Engineering, Polytechnic of Porto
Supervisor
Francisco José Gomes da Silva, PhD
Associate Professor with habilitation, ISEP – School of Engineering, Polytechnic of Porto
Second supervisor
Marcelo Francisco de Sousa Ferreira de Moura, PhD
Associate Professor with habilitation, FEUP – Faculty of Engineering, University of Porto
Examiner
Fábio André Magalhães Pereira, PhD
Assistant Professor, UTAD – University of Trás-os-Montes and Alto Douro>

ACKNOWLEDGEMENTS

Realizar este projeto não teria sido possível sem o apoio e o acompanhamento de algumas pessoas. A elas escrevo aqui o meu mais sincero agradecimento.

Aos meus orientadores, Francisco Silva e Marcelo Moura, que sempre se mostraram disponíveis para rapidamente esclarecer as minhas dúvidas, transmitir os seus conhecimentos e desenvolverem o meu pensamento crítico.

Ao professor Nuno Dourado, por se ter tornado mais do que um orientador. Por me ter permitido integrar o projeto, por todo o esforço que fez para me permitir cumprir os prazos, pelas boleias e por todos os ensinamentos. Às alunas da Universidade do Minho, Teresa Campos e Andrea, por todo o trabalho e dedicação para comigo.

Aos técnicos do ISEP, Víctor Moreira e Vítor Ribeiro e ao engenheiro Hernâni, pelo apoio nas oficinas que permitiu o fabrico dos provetes. Aos professores Fábio Pereira e Cristóvão Santos da UTAD, pela companhia e conselhos transmitidos durante a realização dos ensaios. Ao professor Paulo Nóvoa, do ISEP, pela amabilidade e prontidão para ajudar. Aos médicos Rosmaninho Seabra e Manuel Gutierres, pela ponte que me proporcionaram entre a teoria e a realidade na ortopedia em Portugal.

Ao meu namorado, Rúben Costa, por ter estado sempre presente, pelo apoio, companheirismo, dedicação e debate de ideias.

Queria também deixar o meu agradecimento àqueles que fizeram de mim quem sou hoje, pois sem eles, o meu projeto seria certamente diferente. Aos meus pais e irmã, Céu, José Carlos e Leonor, por me acompanharem todos os dias e pela educação que me proporcionaram.

E a todos que de alguma forma me acompanharam nesta jornada e sempre se fizeram presentes, o meu sincero agradecimento.

Agradeço ainda às instituições Instituto Superior de Engenharia do Porto, Faculdade de Engenharia da Universidade do Porto, Universidade do Minho, Universidade de Trás-os-Montes e Alto-Douro e Faculdade de Medicina da Universidade do Porto, pelo suporte à realização de todo o trabalho.

Este trabalho teve o apoio da FCT – Fundação para a Ciência e Tecnologia, através do projeto com a referência PTDC/EME-SIS/28225/2017, intitulado "Desenvolvimento de um sistema compósito inovador para estabilização de fraturas ósseas cominutivas", com acrónimo "BoFraPla", através do Programa Operacional Competitividade e Internacionalização e o Programa Operacional Regional de Lisboa, apoiada pelo FEDER.

KEYWORDS

Bone tissue; Bone cement; Fracture tests; Pure mode I and mode II; Finite elements; Cohesive models

ABSTRACT

The process of evolution has led to the creation of fantastic materials. Bone is one of these materials and has a complex, anisotropic, hierarchical and heterogeneous microstructure, characterised by an excellent mechanical performance. However, as it is an almost fragile material, it often ends up fracturing. These fractures decrease the patient's quality of life and entail high costs for the health system. In order to deal with these fractures, the BoFraPla project arose, which aims to develop a fibrous system for fixing bone fractures. Therefore, in the scope of the activities of this project, the present dissertation emerges, proposing to mechanically characterise the bond between the bone and bone cement.

From a thorough literature review, it was found that although the bone cement has been used for more than fifty years, there are few references to its mechanical characterisation and none were found that have made a clear characterisation of the fracture process between the bone and the cement. Hence, in this report, a pure mode I characterisation (tension) through a Double Cantilever Beam (DCB) test and another pure mode II characterisation (shear) through an End-Notched Flexure (ENF) test are presented.

In order to overcome the difficulties in monitoring the crack length during the laboratory tests, a method based on the equivalent crack length was used. With this method, the resistance curve was drawn for each specimen and, in most of them, the existence of thresholds was remarkable, which allowed a correct measurement of the fracture energy for each test. In order to validate the results obtained, numerical simulations were performed with cohesive models. Through the results, it was possible to determine that the chosen tests, the defined dimensions and the adopted procedure, can be used to characterise the fracture of these two materials in the studied loading modes.

PALAVRAS-CHAVE

Tecido ósseo, cimento ósseo, testes de fratura, modo I e modo II puros, elementos finitos, modelos coesivos.

RESUMO

O processo de evolução natural levou à existência de materiais fantásticos. O osso é um destes materiais e apresenta uma microestrutura complexa, anisotrópica, hierárquica e heterogénea, caracterizada por um excelente desempenho mecânico. Contudo, como se trata de um material quase frágil, inúmeras vezes acaba por fraturar. Estas fraturas diminuem a qualidade de vida do paciente e acarretam elevados custos para o sistema de saúde. Com vista ao tratamento destas fraturas, surgiu o projeto BoFraPla, que se propõe a desenvolver um sistema fibroso de fixação de fraturas ósseas. Assim, no âmbito das atividades deste projeto, surge a presente dissertação que se propõe a caracterizar mecanicamente a ligação entre o osso e um cimento ósseo.

A partir de uma profunda revisão bibliográfica apurou-se que, apesar do cimento ósseo ser utilizado há mais de cinquenta anos, existem poucas referências à sua caracterização mecânica, não sendo encontrada nenhuma que fizesse uma clara caracterização do processo de fratura entre o osso e o cimento. Assim, neste relatório é apresentada uma caracterização em puro modo I (tensão), através de um ensaio Double Cantilever Beam (DCB) e outra caracterização em puro modo II (cisalhamento), através de um ensaio End-Notched Flexure (ENF).

Para colmatar as dificuldades de monitorização do comprimento de fenda durante os ensaios laboratoriais, recorreu-se a um método baseado no comprimento de fenda equivalente. Com este método foi traçada a curva de resistência para cada provete, sendo notória a existência de patamares na sua maioria, o que permite uma correta medição da energia de fratura para cada ensaio. Com vista a validar os resultados obtidos, foram realizadas simulações numéricas com modelos coesivos. Através dos resultados, foi possível apurar que os ensaios escolhidos, as dimensões definidas e o procedimento adotado, podem ser utilizados para caracterizar à fratura entre estes dois materiais nos modos de carregamento estudados.

SCHLÜSSELWÖRTER
Knochengewebe; Knochenzement; Bruchversuche; Pure Mode I und Mode II; Finite Elemente; Kohäsionsmodelle

ABSTRAKT

Der natürlichen Evolutionsprozess hat zur Entstehung fantastischer Materialien geführt. Knochen ist eines dieser Materialien und weist eine komplexe, anisotrope, hierarchische und heterogene Mikrostruktur auf, die sich durch eine hervorragende mechanische Leistung auszeichnet; da es sich jedoch um ein fast zerbrechliches Material handelt, kommt es häufig zu Brüchen. Diese Frakturen mindern die Lebensqualität der Patienten und verursachen hohe Kosten für das Gesundheitssystem. Um diesen Brüchen zu helfen und sie zu behandeln, wurde das Projekt BoFraPla ins Leben gerufen, dessen Ziel die Entwicklung eines faserigen Systems zur Fixierung von Knochenbrüchen ist. Im Rahmen der Aktivitäten dieses Projekts entstand die vorliegende Dissertation, in der vorgeschlagen wird, die Verbindung zwischen Knochen und Knochenzement, mechanisch zu charakterisieren.

Bei einer gründlichen Literaturrecherche wurde festgestellt, dass der Knochenzement zwar seit mehr als fünfzig Jahren verwendet wird, dass es aber nur wenige Hinweise auf seine mechanische Charakterisierung gibt und dass keine eindeutige Charakterisierung des Bruchprozesses zwischen dem Knochen und dem Zement gefunden wurde. Daher werden in diesem Bericht eine reine Modus-I-Charakterisierung (Zug) unter Verwendung eines Double Cantilever Beam (DCB)-Tests und eine weitere reine Modus-II-Charakterisierung (Scherung) durch einen End-Notched Flexure (ENF)-Test vorgestellt.

Um die Schwierigkeiten bei der Überwachung der Risslänge während der Labortests zu überwinden, wurde eine auf der äquivalenten Risslänge basierende Methode verwendet. Mit dieser Methode wurde die Widerstandskurve für jede Probe gezeichnet, und bei den meisten von ihnen war das Vorhandensein von Schwellenwerten bemerkenswert, was eine korrekte Messung der Bruchenergie für jeden Test ermöglichte. Um die erzielten Ergebnisse zu validieren, wurden numerische Simulationen mit kohäsiven Modellen durchgeführt. Anhand der Ergebnisse konnte festgestellt werden, dass die gewählten Versuche, die definierten Abmessungen und das angewandte Verfahren zur Charakterisierung des Bruchs dieser beiden Materialien bei den untersuchten Belastungsarten verwendet werden können.

LIST OF SYMBOLS AND ABBREVIATIONS

List of abbreviations

AFPB	Asymmetric Four Point Bending test
BCS	Bilayer Compact Sandwich
CBBM	Compliance Based Beam Method
CPC	Calcium phosphate cements
CS	Compact Shear Test
CT	Compact Tension Test
CZM	Cohesive Zone Model
DCB	Double Cantilever Beam
DIC	Digital Image Correlation
ELS	End Loaded Split
ENF	End-Notched Flexure
EPFM	Elastic-Plastic Fracture Mechanics
i.e.	*Id est* (this is)
FCT	Fundação para a Ciência e Tecnologia (Portuguese national funding agency for science, research and technology)
FM	Fracture Mechanics
FPZ	Fracture Process Zone
ISEP	School of Engineering, Polytechnic of Porto
ISO	International Standards Organisation
LEFM	Linear Elastic Fracture Mechanics
NLFM	Nonlinear Fracture Mechanics
SENB	Single Edge Notch Beam
UTAD	University of Trás-os-Montes and Alto Douro
vs	Versus
X-FEM	Extended finite element method

List of units

°C	Degree Celsius
g	Gram
GPa	Gigapascal
h	Hour
m	Metre

min	Minute
mm	Millimetre
MPa	Megapascal
N	Newton

List of symbols

%	Percentage
a	Crack length [mm]
a_0	Initial crack length [mm]
a_e	Equivalent crack length [mm]
A	Cross sectional area [mm^2]
B	Specimen width [mm]
C	Compliance [mm/N]
E	Young's modulus [MPa]
E_f	Equivalent flexural modulus [MPa]
E_L	Longitudinal Young's modulus [MPa]
G	Energy release rate [N/mm]
G_c	Critical strain energy release rate or fracture energy [N/mm]
G_{Ic}	Mode I fracture energy [N/mm]
G_{IIc}	Mode II fracture energy [N/mm]
G_{LR}	Shear modulus in the LR plane [N/mm]
h	Thickness [mm]
I	Second moment of area [mm^4]
k	Interface Stiffness [N/mm^3]
K	Fracture toughness [$MPa\sqrt{m}$]
L	Specimen length [mm]
P	Load [N]
P_{max}	Maximum load [N]
U	Speed [mm/s]
w	Crack opening displacement [mm]
α	Stress ratio
β	Displacement ratio
δ	Displacement [mm]
v	Poisson's ratio
σ	Local stress [MPa]
σ_{max}	Maximum stress [MPa]
Υ	Exponent value from the power law energy-based criterion

GLOSSARY OF TERMS

Anatomy	Science that studies the structural organisation of living beings, including the systems, organs and tissues which constitute them, the appearance and position of the various parts, the substances they are made of, their location and their relation to the remaining parts of the body.
Angiogenesis	Term used to describe the growth of new blood vessels from existing ones.
Distal	In anatomy, the term distal is used to indicate the part of the body, which is furthest from a centre. Distal is the opposite of proximal and refers to distance.
Delayed bond	Bond in which the fracture repair exceeds the expected healing time.
Dislocation	Sudden displacement of one or more bones in an articulation.
Bone non-union	Ceasing of the bone healing process.
Proximal	In anatomy, the term proximal is used to indicate the part of the body that is closest from a centre.
Toughness	Property of a material, which quantifies its resistance to the initiation and propagation of cracks, that is, the aptitude of the material to absorb energy until its rupture.

FIGURES INDEX

TABLES INDEX

INDEX

INTRODUCTION

1 INTRODUCTION

It is estimated that, in the world, approximately 27 million people access hospital emergencies every year (about 37% of visits), and 1.9 million need to be hospitalised as a result of bone fractures [1]. These can occur because of road accidents, agricultural and industrial accidents, cases associated with violence, falls, sports, among others [2]. In fact, the incidents that induce traumatic injuries are immense and these are the fourth leading cause of death in the world, being the main cause for ages between 1 and 44 years. Also, when they are not fatal, they sometimes lead to a reduction in the patient's quality of life and high costs, both for the health system and for society in general [1]. Precisely, due to these statistical data, there is an immediate need to act in this sector and develop solutions to control and reduce the risks of death, or increase the quality of life of people who suffer from this category of injuries. There are several types of traumatic injuries: dislocation, contusion, sprain and fracture. Dislocations and sprains occur in the articulations, contusions at the level of soft tissues and fractures at the level of bones.

The present work is dedicated specifically to the study of fractures. In this context, it is essential to study and characterise the behaviour of bone with fixation systems in order to develop solutions which enable a better quality of life for patients and to reduce the socioeconomic impact of expenses caused by the bone fracture treatment systems currently used. This dissertation is intended to contribute towards the meeting of these needs, specifically in the study of the mechanical behaviour of the bond between bone and bone cement.

Next, a brief contextualisation of the project in which the dissertation is inserted is carried out, followed by the presentation of its objectives and methodologies and, finally, a presentation to the organisation of this report.

1.1 Framework

This dissertation was developed within the scope of the master’s degree in mechanical engineering – materials and manufacturing technologies branch of ISEP. It was developed by Marta Luísa Sousa Barbosa, with a bachelor’s degree in biomedical engineering from the same institution, under the guidance of Professor Francisco José Gomes da Silva and Professor Marcelo Francisco de Sousa Ferreira de Moura.

The work developed here is part of the activities of the ongoing research project, BoFraPla, financed by FCT (Fundação para a Ciência e Tecnologia – Portuguese national funding agency for science, research and technology). The project aims to develop an innovative fibrous system for stabilisation of comminuted bone fractures.

The challenge proposed for this work consists in the collaboration in some tasks inherent to the project, namely the fracture characterisation in pure mode (I, II) of bonded joints between cortical bone tissue and bone cement. This task is of the utmost importance in the scope of the project, since the fibrous system under development will be fixed to the bone tissue using bone cement and, as such, it is necessary to know the fracture behaviour of this compound.

1.2 Objectives and work steps

The main objective of this dissertation is to develop methodologies and procedures appropriate for fracture characterisation of bonded joints with cortical bone tissue and bone cement. Thus, this dissertation is divided into three large groups and each one of them presents its own work steps.

- **Background**
  - To know the bone tissue and the bone cement;
  - To identify the main bone fractures and the modes of propagation of cracks;
  - To distinguish the loading modes and the associated basic mechanical tests;
  - To study the mechanical tests DCB and ENF, and find out references in the literature to their application in bones;
  - To determine the different modes of treatment to bone fracture.
- **Laboratory component**
  - To manufacture specimens;
  - To perform DCB and ENF tests;
  - To develop methodologies and procedures appropriate for fracture characterisation of bonded joints with cortical bone tissue and bone cement;
  - To obtain G_{Ic} and G_{IIc}.
- **Numerical component**
  - To apply finite element methods;
  - To validate the experimental procedures.

1.3 Methodology

The methodology followed in the developed work is:

- **1. Project integration**
    - Phase that consisted in the project integration, alongside the learning of theoretical concepts related to it.
- **2. Problem analysis and definition of the objectives**
    - Stage dedicated to the definition and delimitation of the activities to develop during the project, in order to identify the objectives of the work.
- **3. Bibliographical research**
    - In order to gather the information presented in this report, two different methodologies were used. The first one consisted in an in-depth bibliographic review, in technical books or scientific articles, mostly present in ScienceDirect and PubMed databases, about topics considered relevant for the development of the laboratory and numerical component. The second approach consisted of interviews with reference professionals to find out whether the information described in the literature is currently used in practical terms in Portugal.
- **4. Specimens' manufacturing**
    - This stage was dedicated to the definition and construction of the specimens to be used in the experimental tests.
- **5. Performance of the tests**
    - In this stage, the two proposed fracture tests (DCB and ENF) were performed.
- **6. Processing of the results**
    - The data obtained from the experimental tests were analysed and worked on in order to draw conclusions.
- **7. Validation of the processing procedure**
    - The Abaqus® software was used to run finite element routines and confirmed the laboratory procedures.

1.4 Structure of the report

This report contains five main chapters, which are divided as follows:

- **1. Introduction**
    - Framework: Presents a short contextualisation of the work;
    - Objectives: Includes the objectives of the present project;
    - Methodology: Briefly describes how to obtain the content present in the document;
    - Structure of the report: Schematises the organisation of the present report.

- **2. Background**
    - Orthopaedic anatomy: Describes the bone tissue;
    - Bone fractures: Exposes the main bone fractures, the fracture modes and some fracture mechanic tests;
    - Application of finite element analysis to bone fracture: Introduces concepts of the finite element method.
- **3. Development**
    - Experimental component: Describes the specimens' manufacturing and the mechanical tests;
    - Numerical component: Validates the experimental component.
    - Results: Presents both experimental and numerical results
    - Discussion of results: Discusses the results obtained
- **4. Conclusions**
    - Includes the conclusions obtained with the development of this work.
- **5. Bibliography**
    - Presents the sources of the exposed content.

BACKGROUND

2.1 Orthopaedic anatomy

2.2 Bone fractures

2.3 Application of finite element analysis to bone fracture

2 Background

After a bone fracture, it is most often necessary to apply a support or replacement system to the damaged bone structure. In order to apply the system correctly and to promote the best possible performance, it is extremely important to predict the future performance of that system. This depends on the forces to which the system is subjected, the loads imposed on each of the materials which constitute it and the strength of these materials to the loads throughout the expected lifetime [3]. Thus, in this chapter, a review of the literature regarding bone characterisation is performed.

2.1 Orthopaedic anatomy

The skeleton is an elementary structure responsible for multiple functions, among which the structural function stands out. Moreover, besides allowing the protection of internal organs, also enables locomotion [4], [5]. The human skeleton is made up of 206 bones, which are some of the most consistent structures of the body (only surpassed by dentine and enamel) [3]. Besides their high hardness, bones present a complex, anisotropic, hierarchical and heterogeneous microstructure, being one of the most dynamic and metabolically active tissues [3], [6], [7]. Its dynamism is due to its growth and regenerative capacity, which allows them to repair and form new bone when some injury occurs. In addition to these characteristics, bone tissue has the particularity of being considered both an anatomical structure and a physiological organ.

Figure 1 summarises the concepts related to bones and which will be explained throughout this sub-chapter.

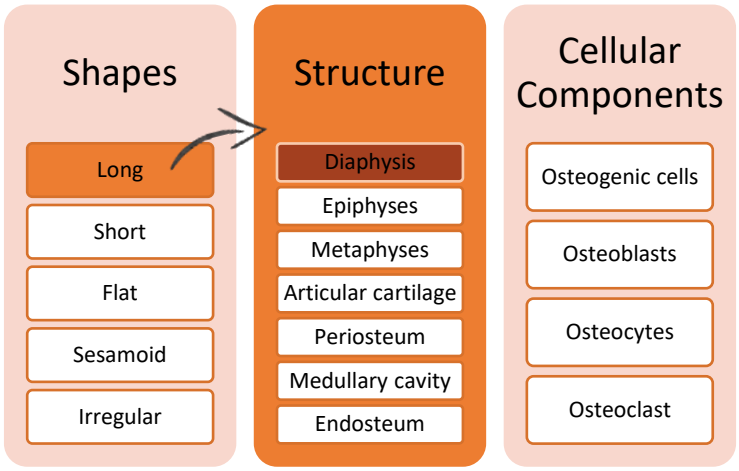

Figure 1 – Summary diagram of bone characteristics

Regarding the classification by shape, there are different categories of bones. As summarised in Figure 1, there are [1], [5]:

- Long bones (Figure 2) – those that possess a length which is greater than the thickness and width;
- Short bones – those that have a cubic shape with approximately equal length and width;
- Flat bones – those that are generally thin and present extensive areas for muscular insertion and protection;
- Sesamoid bones – those that are generally small and triangular or more circular in shape; but, as the name indicates, are close to the shape of sesame seeds, and have the function of protecting the tendons from excessive wear and tear;
- Irregular bones – these are the remaining bones that cannot be grouped in any of the other categories.

Figure 2 shows the typical structure of a long bone, being all its constituents represented as well.

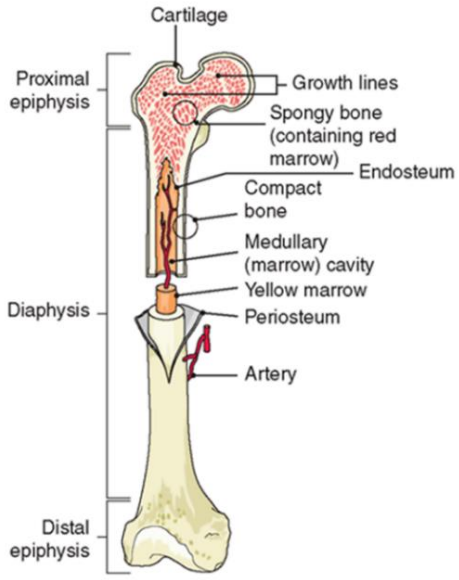

Figure 2 – Structure of a long bone (adapted from [8])

As for their structure (Figure 1 and Figure 2), the long bones, objective of this work, are typically composed of seven different constituents. These constituents are [1], [5], [9]–[11]:

- Diaphysis – a long, roughly cylindrical shaft formed by a thin, dense outer layer of compact bone surrounding the cancellous bone;
- Epiphyses (the proximal and the distal) – the extremities of the bone;
- Metaphysis – these correspond to the area between the epiphysis and the diaphysis;
- Articular cartilage – a thin layer of cartilage that covers the epiphysis, reducing friction and absorbing shock on impact with other bones;

- Periosteum – fibrous layer that covers the connective tissue layer protecting the bone, nourishing it, assisting in fracture repair and enabling fixation for ligaments and tendons;
- Medullary cavity – circular-shaped hollow space located inside the diaphysis which contains yellow bone marrow;
- Endosteum – thin membrane that coats the internal bone surface.

The present dissertation operates at the level of the diaphysis.

The compound structure and the complex hierarchical organisation of the bone range from the macroscale to the atomic scale and, therefore, make it a fascinating material with much still to be discovered. Figure 3 shows a representation of the bone from the macroscale to the nanoscale.

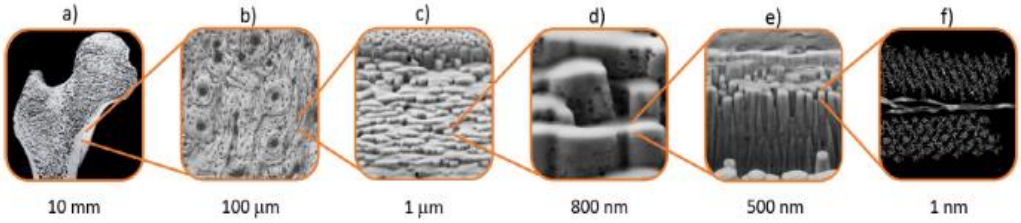

Figure 3 – Representation of the bone from the macroscale to the nanoscale [12]

From a histological point of view, bone tissue is only a specialised form of connective tissue, which, like the other similar tissues, is essentially formed by cells (inorganic part), an extracellular matrix (organic part) and water [3], [9], [13]. From a microscopic point of view and focusing on cortical bone tissue, the bone is formed by osteons, which exhibit channels, the Havers' channels, and a complex lamellar matrix, forming a characteristic pattern. Thus, as it can be seen in Figure 4, around each Havers' channel there are lamellae. The lamellae are formed by collagen fibres that have small gaps which house bone crystals, such as hydroxyapatite and bone cells [7], [10].

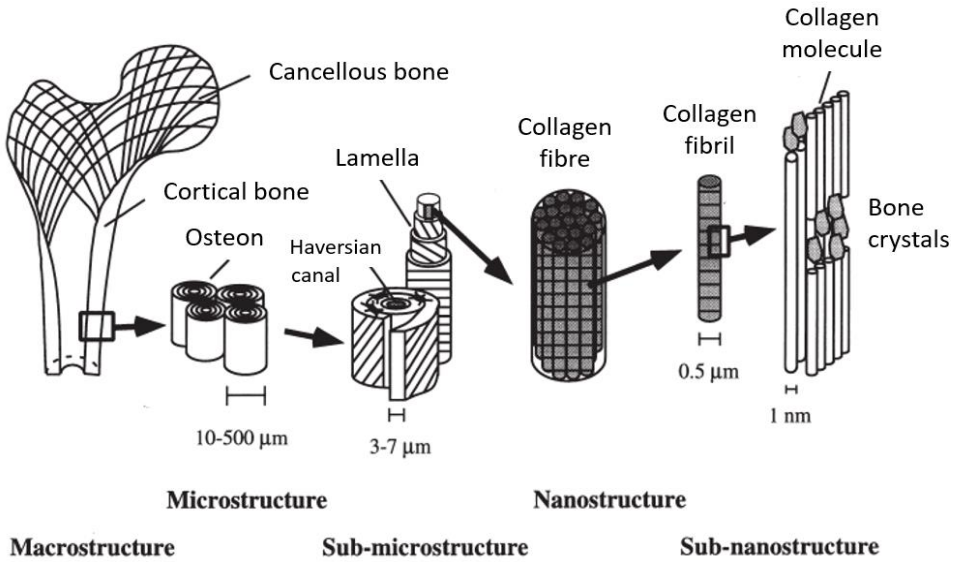

Figure 4 – Schematic of the microstructure of the cortical bone tissue [7]

As described in Figure 1, there are four types of cells present in bone tissue [1], [4], [10], [11], [14], [15]:

- Osteogenic stem cells are mesenchymal stem cells which, as their classification indicates, are undifferentiated and have the capacity to differentiate into different cell types, allowing a functional reconstitution of certain tissues;
- Osteoblasts are bone-forming cells, i.e., they play an important role in synthesis and mineralisation of the matrix, in the initiation of the bone reabsorption process and in the interaction with osteocytes;
- Osteocytes are inactive osteoblasts responsible for maintaining the integrity of the bone matrix;
- Osteoclasts are cells that act in the bone destructive processes, whenever its renewal or remodelling is necessary.

Although there are these four cell categories present in the bone, various authors (as is the case of Stell [10] and Ebnezar [1], for example) only refer to the existence of three, since they do not consider osteogenic stem cells as a cell type. This consideration is understandable since it is the osteoblasts, osteocytes and osteoclasts that are the osteogenic cells responsible for bone transformation and remodelling [4].

Bone is constantly undergoing osteoblastic formation and osteoclastic reabsorption, which allows continuous bone remodelling. Thus, there is an extremely well-developed system that maintains normal bone homeostasis and helps in the bone's remarkable ability to self-heal [4].

Bone is a structural and natural composite between ceramics and polymers [9] that has an abundance of mineral salts. Calcium phosphate is the most abundant and combines with calcium hydroxide to form hydroxyapatite crystals. These crystals, in their formation, combined with other salts, such as calcium carbonate, magnesium, potassium, fluoride and sulphate. All these salts, when deposited on the collagen fibres of the extracellular matrix, crystallise and harden the tissue. This crystallisation process is called calcification and is initiated by osteoblasts [5]. Crystallisation is important both to propitiate bone growth and to repair fractures.

Figure 5 visually represents the distribution of bone tissue constituents and, as can be seen, its main constituent is the mineral bone, which is essentially formed by hydroxyapatite. The second-largest constituent is the extracellular matrix, i.e., the organic matrix, mostly formed by collagen and, to a lesser extent, by proteins. Mineralisation provides high stiffness and resistance, while the collagen matrix provides malleability and toughness.

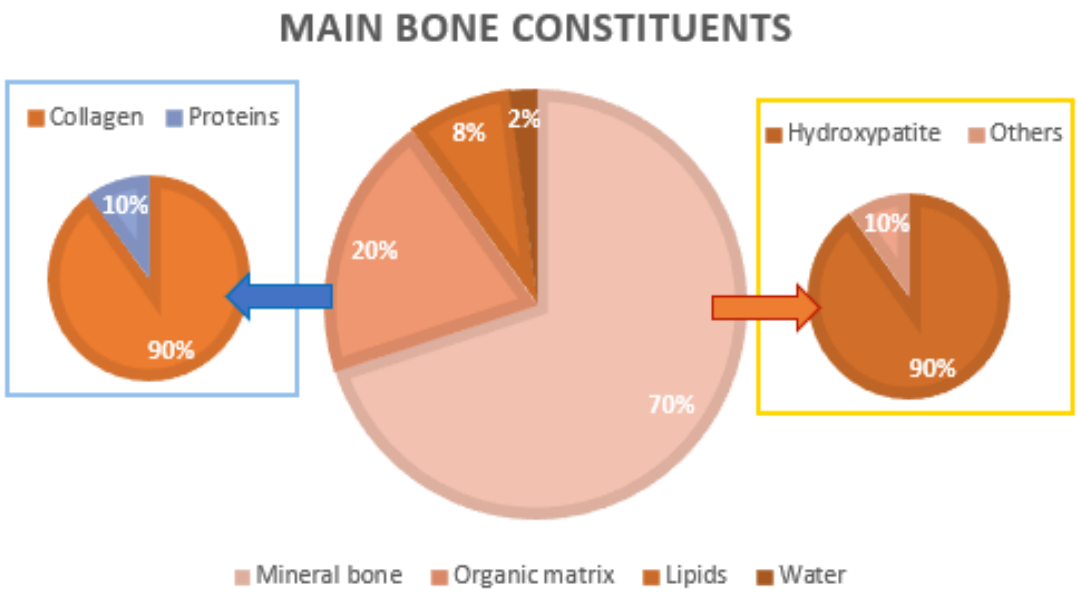

Figure 5 – Distribution of the main bone constituents (adapted from [3])

Hence, these combinations give bone tissue unique properties that provide an excellent resistance to mechanical stress, with the possibility of extension and compression [16], [17]. The percentages indicated in the scheme are not exact for all individuals, but are instead average values, since the percentage of minerals in the bones rises and the percentage of organic matrix reduces as the individual's age increases [3], [18], [19].

Emphasising the great complexity of this tissue, it is possible to observe changes in bone density when loads are administered or removed, and changes in shape due to fracture healing or certain surgical interventions [3].

Among the main properties of the skeleton, those of structural support and metabolic reserve have a special prominence and are normally in stable equilibrium; however, in the case of alteration in this equilibrium, the structural function is always sacrificed in favour of the metabolic one [16]. This sacrifice causes a variation in the bone constitution and, consequently, an alteration in the mechanical properties, i.e, as the structural function is sacrificed, certain diseases begin to appear, such as osteoporosis, which causes the appearance of pores in the bone and thus a decrease in its mechanical resistance [18].

In summary, the bone is an extremely resistant, light, adaptable and multifunctional material, characterised by an excellent mechanical performance [12].

2.2 Bone fractures

There are certain problems that influence the behaviour of the bones and their ability to continue to fulfil their functions. These include congenital, hormonal and metabolic problems, or tumour conditions, for example. However, in these situations, little or

nothing can be done, and they rarely occur. Consequently, traumatic injuries are the main focus of research [1].

In the book by Orozco and his team [20], a review of more than fifty-four thousand fractures of long bones is presented and, of these, more than 30% correspond to fractures in the diaphysis of the analysed bones. This type of injury is one of those with the highest incidence, only surpassed by fractures of the proximal epiphysis of the femur (area close to the union between the femur and the hip), which alone account for around 42% of the fractures. Therefore, the relevance of studying bone fractures in the diaphysis of long bones can be understood.

Diaphyseal fractures (Figure 6) in cortical bone show some similarity to macroscopic fractures of glass and ceramics. Long bones broken in pure bending may show overhanging undulation, in pure torsion a helical fracture may be evident and higher energy fractures (regardless of loading mode) cause crack branching and multiple fragment formation (also known as comminuted fractures). However, unlike glass and ceramics, bones exhibit limited plasticity (and are even considered quasi-fragile), so a quantitative analysis of the surface characteristics should be applied with caution [9].

Figure 6 – Diaphyseal fracture seen by x-ray analysis [21]

The classification of a fracture is of particular importance, since it allows defining, characterising and providing information on the treatment method of the respective fracture. The importance of this method was understood early on and began to be used. *Edwin Smith Papyrus* (XVII b.C.) already presents a classification of fractures, although it is very rudimentary. In this document, it is stated that if there was a fracture with “an injury over it, perforating” (currently called an open fracture), “it should not be treated” [22]. Therefore, as it is perceptible, this first form of

classification served both to define the fracture and to indicate its treatment. Currently, there are multiple forms of classification (some more accepted than others); however, the idea of all classification systems remains, that is, they serve to define fractures as to their characteristics, indicate treatments and predict the treatments' results.

According to one of the most accepted forms of classification for long bones (Müller classification [23]), diaphyseal fractures of long bones are divided into three categories (A, B e C), indicating increasing severity. Besides the classifying letter, Müller adds a colour system like a traffic light, where, once more, the colour is associated with the severity of the fracture. Figure 7 represents three images of bone fractures, one of each of the categories defined by Müller. In the left image (A), a type-A fracture is represented, a simple fracture, i.e., that only divides the bone in two segments. In the right image, (C), a complex fracture is represented, that is, with multiple segments. As for the middle image, (B), an intermediate level fracture is found [1].

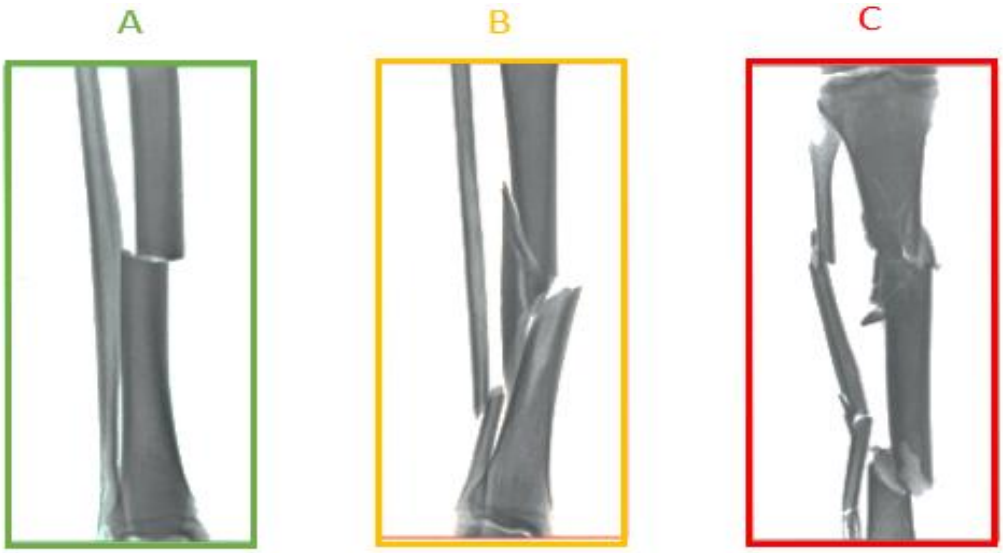

Figure 7 – Illustrative image of fractures classified according to Müller's classification [20]

Essentially due to their main structural function, bones are constantly subjected to the most varied categories of stresses, showing a behaviour very similar to a structure developed by engineering processes [24]. The basic types of application forces (compression, tension, torsion and bending) perform a predictable behaviour in the bone. As expectable, a compressive force shortens the length of the bone, while a tension one lengthens it, a torsional force causes rotation around its axis and the bending bends it in the central zone. A fracture is the result of the structural failure of the bone by means of applied forces, i.e., when the stress placed on the bone is such that causes it to deform beyond its elastic limit and, consequently, to break [25]. This results in characteristic fracture patterns that allow the identification of the type of load that was applied in excess at the time of the fracture [6].

Figure 8 depicts a scheme, which relates the type of load applied to a bone with the correspondent fracture pattern caused.

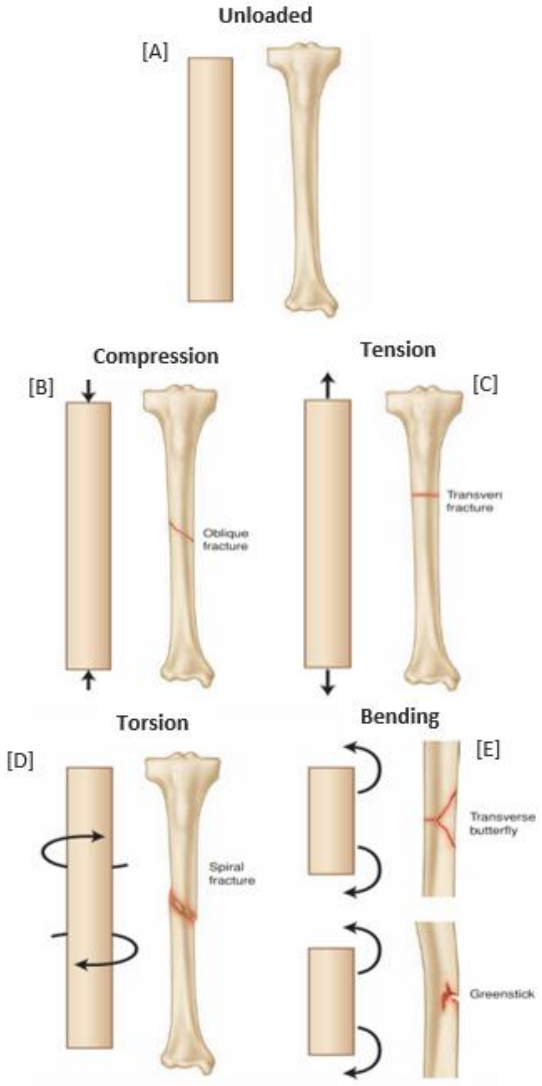

Figure 8 – Different loads and their types of fracture (adapted from [6])

As may be seen in Figure 8, without any load (Figure [A]), no fracture occurs. Considering a compressive force (Figure [B]), oblique fractures are originated, since due to the orientation of the fibres, the bone is less resistant in shear than in compression. With tensile forces (Figure [C]), transverse fractures take place and with torsion forces (Figure [D]), spiral fractures are formed. When bending forces are applied (Figure [E]), these cause compression stresses on one side, and tensile stresses on the other. Consequently, partial fractures may occur, which are common in paediatrics and called “green branch” fractures or fractures that are a junction between an oblique and a transverse fracture, the so-called butterfly fractures [6]. It is important to note that, in a real context, there may not be only one type of force acting solely, therefore fractures may arise with patterns that are a mixture of these.

As explained in the previous paragraph, the force needed to fracture a bone can produce different effects, according to the categories of the force; however, the

intensity itself can also give different results and, depending on its own characteristics, the results can be different as well. For example, the stiffness of the bone varies according to its density. Thus, with the decrease in density (common with age or certain pathological diseases), its stiffness decreases and, consequently, the resistance of the bone to the application of stresses also reduces. Therefore, it is more prone to fracture with forces of lower intensity when compared with high density bones.

Besides these traumatic fractures in which it is necessary to apply a load above the tolerable level, bones are subjected to fatigue. This condition, defined as originating from cyclic repetitions and without the occurrence of trauma, manifests itself in the form of micro-cracks that can evolve into fractures [26]. Fatigue failures in the bones may occur as a result of very frequent loading or exceptionally high-stress amplitudes. The information that is currently available on fatigue failure in bones comes mostly from the engineering materials knowledge [27].

Since 1960, it has been observed that the bone contains many small cracks [28] and that the size of these cracks increases both after fatigue loading and in older people [29], [30]. The work of O'Brien's team in the 2000s made it possible to label bone microcracks and thus enabling a more systematic study to understand how microcracks interact with the surrounding microstructure. With these studies, it was found that the cracks grow relatively quick until they reach lengths of around 100 µm, where they tend to stop. The reason for their stop at this location is that they encounter osteon boundaries, whose act as barriers to the continuity of propagation [31], [32].

The beginning of sudden crack growth in bones is related to a key parameter called "fracture toughness". This parameter measures the resistance of the bone material to crack propagation [33]. Hence, in a general way, the fragility of the bone can be defined as the susceptibility to the occurrence of fractures, and the resistance of these fractures depends, as expected, both on the properties of the constituent materials and on the structural properties themselves. Figure 9 represents the fracture toughness parameter.

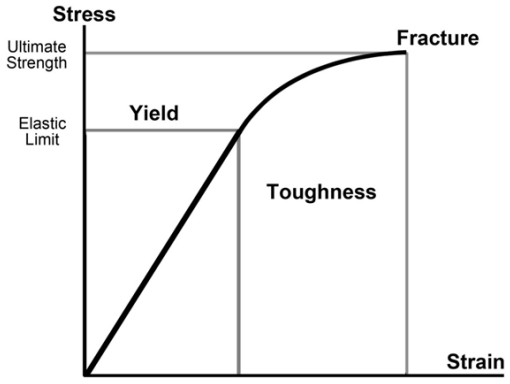

Figure 9 – Area corresponding to fracture toughness in a stress-strain graph [34]

Several studies refer to the application of elastic-plastic fracture mechanics (EPFM) concepts as an approach that allows the evaluation of both the elastic and plastic part

of the energy dissipated during bone fracture [12], [35], [36]. Nevertheless, most current applications of Fracture Mechanics (FM) are limited to the use of Linear Elastic Fracture Mechanics (LEFM). Norman and his team [37] considered the concepts of this technique and performed a Compact Tension (CT) test to compare the fracture toughness of human and bovine bones, analysing several aspects in order to determine their contribution to fracture toughness. However, the authors admit a malfunction of LEFM approaches since the value of the energy release rate, G, increases with crack propagation and never stabilises. Yang and his team [38] tested humerus cortical bone also with the CT testing and considered two different approaches: LEFM and nonlinear fracture mechanics (NLFM) considering a cohesive zone model (CZM). The authors observed that the LEFM was unable to mimic load-displacement curves, but the nonlinear model was able to predict several load-displacement curves after calibration with data from one curve. Thus, the authors state that LEFM is not an accurate model to be applied to cortical bone tissue and the nonlinear CZM is a more accurate approach to predict bone fracture behaviour.

As a consequence of its microstructure and the interaction between its constituents, bone fracture reveals some damage mechanisms in the proximities of the crack's end. These mechanisms, such as micro-cracks, crack deflection and fibre bridging, are responsible for the development of a non-negligible fracture process zone (FPZ), which means that the LEFM theory does not apply [7], [39].

For this reason, the resistance curve method (*R*-curve) becomes the best method to determine bone toughness. In this method, the evolution of the fracture energy is described as a function of the damage progression [40]. Several authors refer to the use of the *R*-curve method in their articles on bone mechanical tests [41]–[44]. In Figure 10 these fracture toughness mechanisms are represented.

The primary intrinsic mechanism (Figure 10 [d]), i.e., the one that acts ahead of the crack's end and originates the crack initiation toughness, appears to be due to the plasticity created by sliding collagen fibrils or other deformation mechanisms and acts at the sub-micrometre scale, contributing to a resistance of the order of 1-2 MPa$\sqrt{\mathrm{m}}$ in normal and healthy bones. On a slightly larger length scale, another intrinsic mechanism operates, the micro-crack (Figure 10 [b]). It is thought that the formation of a large cloud of micro-cracks ahead of the main crack may function to consume energy and create compressive residual stresses as a result of the volume change involved. As the crack extends, two important extrinsic damage mechanisms operate: crack bridging (Figure 10 [c]) and crack deflection. The bridge arises because, as the crack propagates, it leaves a trail of some whole osteons, which, as they have not been ruptured, they transmit some force through their ligaments, reducing the intensity of the stress at the crack's end. In normal bones, this mechanism can increase the toughness by several MPa$\sqrt{\mathrm{m}}$ above the intrinsic value. Crack deflection (Figure 10 [a])

generally occurs at the interfaces between lamellae and at the surfaces of the osteons [27].

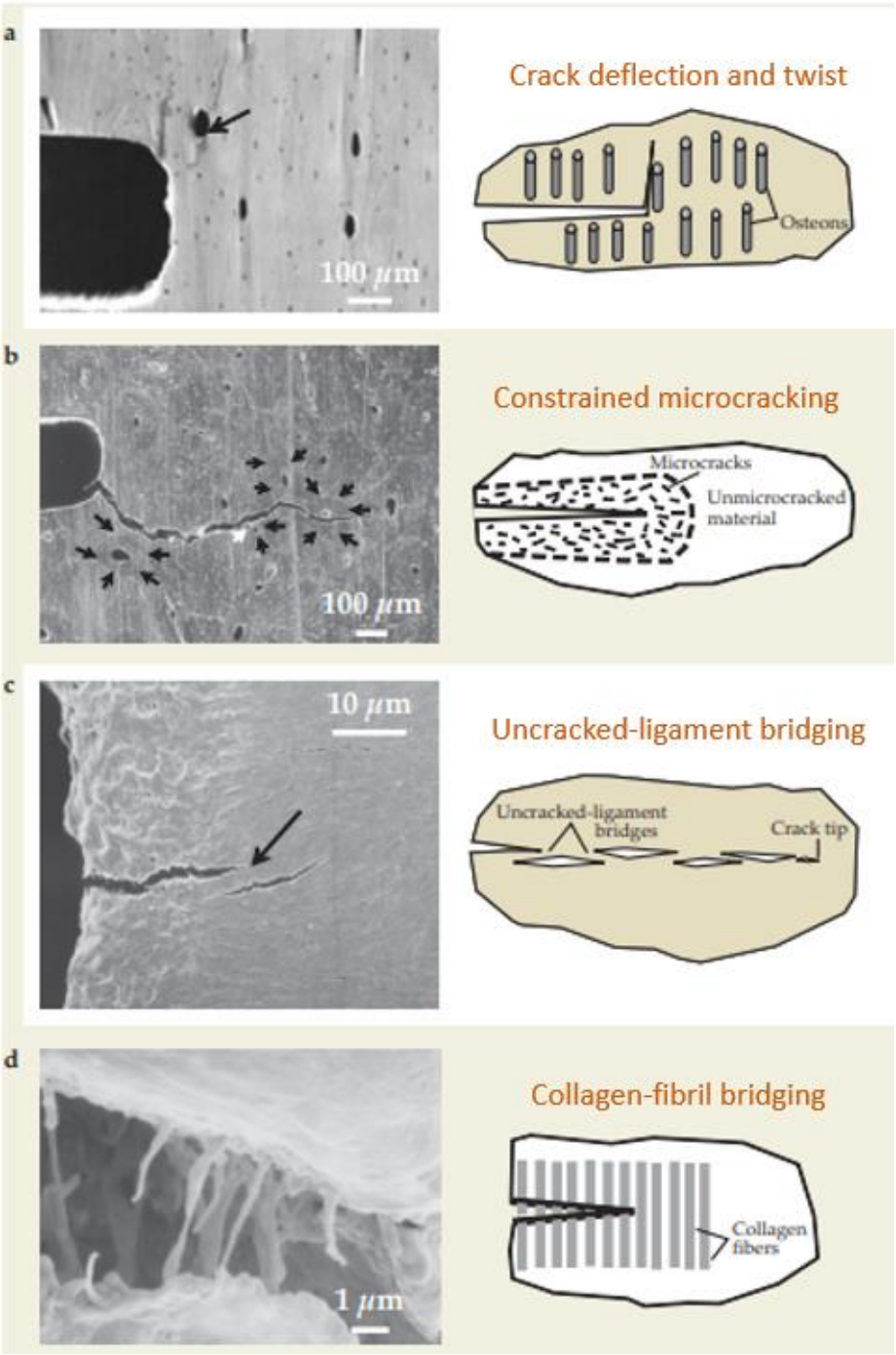

Figure 10 – Fracture toughness mechanisms [45]

Due to this great variability of characteristics, almost unique to each individual, the study of bone fracture becomes an important research topic, since it may contribute to the understanding of the fundamentals of bone insufficiency induced by diseases, as well as by age, medication or physical exercise activities [40].

2.2.1 Fracture concepts

Fracture mechanics (FM) is an area that aims to characterise the fracture behaviour of materials and assumes that a structure is not necessarily a continuous medium, therefore it may possess defects caused, for example, by the manufacturing process [46], [47]. According to this area, there are two main types of criteria to predict the propagation of a crack. The first is based on the energy release rate and the second is translated into the stress intensity factor. However, it is important to note that the two criteria are related and are properties of the material [47]. The most used criterion in heterogeneous materials, as is the case of bone tissue, is based on the G value. It considers that the propagation of an internal defect will occur when the energy available at the end of that defect (value of the strain energy rate – G) equals the energy necessary for the crack propagation (critical energy release rate – G_c) [47], [48].There is some work developed through the use of FM approaches to understand bone failure, either to try to comprehend fracture development and growth, or to study the effect of the microstructure of this element on toughness resistance. Most of the studies presented in the literature use cadaver tests, which is expected, since most of them are destructive tests. There is a wide variety of types in what concerns the origin of the bones tested and the literature also reveals that bones from different animal species are similar to human ones. There are tests to determine bone fracture toughness in animals such as rabbits [49], bovines [50], [51] or horses [41], for example.

There is a large scatter of bone mechanical properties present in the literature, which is justified by reasons presented in Figure 11. Wolff's law, first presented at the end of the 19th century by Julius Wolff (German physiologist), aims to describe how the bone adapts itself to a load imposed on it. This law states that the lamellae of the bone are not only designed to provide support, but also to respond to the tensions imposed on them and are, therefore, constantly changing their structural constitution [52]. This change in the constitution causes tests performed on specimens taken from one individual to show considerably different values when compared to another individual. In addition to this, as the lamellae are preferentially aligned in the direction of the maximum stresses applied, there is an anisotropic distribution of resistance and stiffness in relation to the considered direction. Cortical bone samples present three orthogonal directions, which are defined in Figure 12. It can be seen that the Young's moduli E_i Poisson's ratios ν_{ij}, and shear moduli G_{ij} (i, j = L, T, R) measured along the longitudinal axis (direction L) differ significantly from the radial (direction R) and circumferential (direction T) directions. Direction L reveals much higher values in comparison to the others, which present similar values [9].

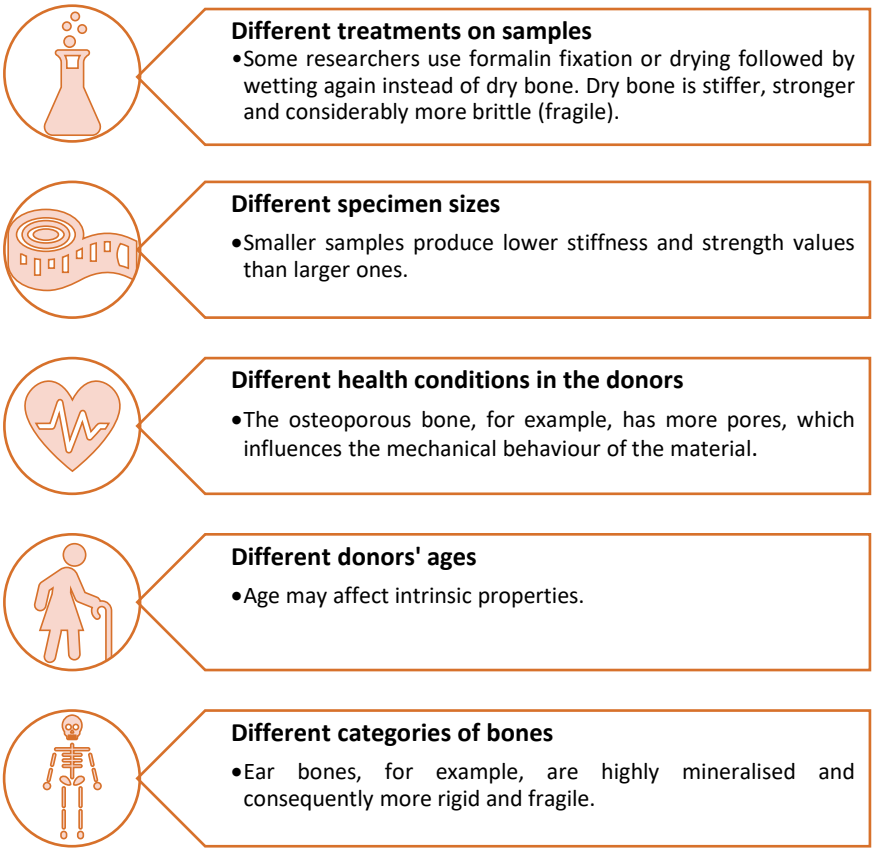

Figure 11 – Reasons for the variety of mechanical properties of tested bones (adapted from [53])

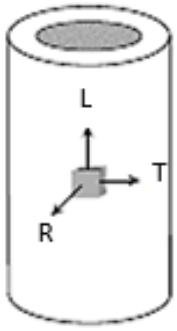

Figure 12 – Cutting directions of specimens (adapted from [9])

Concerning the stiffness, there are three ways to test bones: mechanically (relating tensions with deformations), optically and ultrasonically (submitting the bone to ultrasound and measuring the sound's velocity). In this dissertation, the only adopted method is the mechanical approach.

In order to have an idea, Table 1 presents the human femur's elastic properties experimentally obtained by Ashman and his team [54].

Table 1 – Elastic properties of the human femur (values in GPa)

E_R	E_T	E_L	ν_{RT}	ν_{RL}	ν_{TL}	G_{RT}	G_{RL}	G_{TL}	Source
20.0	13.4	12.0	0.35	0.37	0.42	6.2	5.6	4.5	[54]

As shown in Figure 13, fracture characterisation tests are divided into three possible loading modes. Mode I applies to tension loading and modes II (shear) and III (tearing), on their behalf, apply to shear solicitations. In bones, although tension loadings seem to be the most common, in twisting or torsion efforts during normal activities, for example, bone fractures can occur under pure shear loading too [55]. Nevertheless, in practical terms, bone materials in the skeleton are subjected to multi-axial loads and the fracture phenomenon usually occurs in mixed-modes I+II [33]. Furthermore, the anisotropy induced by the alignment of osteons along the long bone axis promotes confined regions and, as such, prone to define crack propagation paths in pre-established regions and consequently to develop mixed-mode fracture conditions [40].

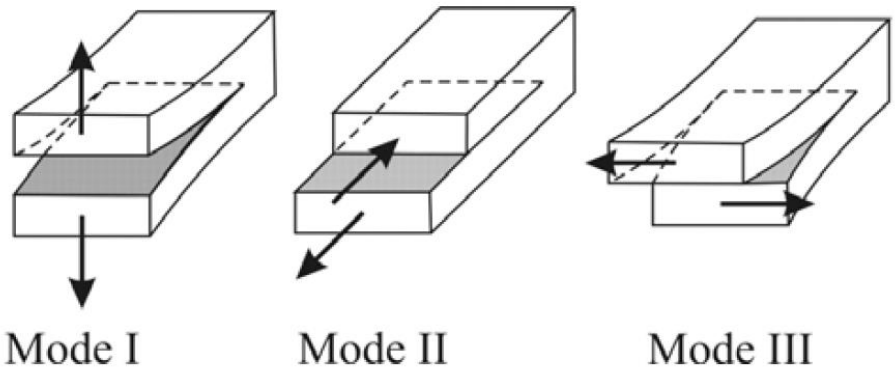

Figure 13 – Types of loading modes [48]

2.2.2 Fracture tests

Bone has certain mechanical properties that can be measured. These, as seem before, include the amount of deformation when a load is applied to it, the mechanism and the speed with which damage accumulates or propagates, and the maximum loads that it can withstand. To determine these properties, laboratory tests are applied which consist of applying well-defined loads under controlled and previously established conditions.

Most of the studies present in the literature regarding bone fracture characterisation are on pure mode I loading. Articles with several tests can be found, among which the Compact Tension (CT) [30], [37], the Single Edge Notch Beam (SENB) [35], [56]–[59] and the Double Cantilever Beam (DCB) [9], [44], [56], [60], for instance. Some authors, such as Koester *et al*. [58] recognise that bones are not only subjected to pure mode I and, therefore, they present both pure mode I and pure mode II tests in the same paper. Koester and his team analysed environmental scanning electron microscopy images of human cortical bones under pure mode I and pure mode II fractures and studied the fracture path propagation for both modes. Nonetheless, it must be recognised that much less attention has been devoted to mode II bone fractures, essentially due to experimental difficulties, namely defining a suitable test method [40]. In fact, the characterisation of mode II fractures acquires special relevance for

different reasons, among which the evidence that bones are subjected to pure shear loading, as is the case of torsional efforts [55]. In pure mode II, the End-Notched Flexure (ENF) [61], the End Loaded Split (ELS) [61], the Compact Shear (CS) [37] and the Asymmetric Four-Point Bending (AFPB) [62] tests are found.

According to Morais *et al*. [44], the DCB test possesses several advantages in comparison to other geometries (such as the CT test or SEN, for example) to obtain bone fracture characterisation on pure mode I loading. Effectively, given the existence of an extensive fracture process zone in the cortical bone tissue, the DCB test allows a more stable crack growth to occur, and therefore providing an adequate self-similar propagation and avoiding spurious effects in the fracture energy measurements.

As for the mode II tests found, Pereira *et al*. [40] performed a numerical analysis of the CS test proposed by Norman [37] and found that this test presents some difficulties regarding the exact measurement of fracture energy under pure mode II loading. Pereira's team states that, in order to use this test, it is necessary to use at least long bone samples to guarantee a reliable estimation for bone fracture energy. Either due to the difficulty in working bones or due to the very limitations of the dimensions of the material, this may be a difficult test to achieve. The same team [40] also contests the AFPB test proposed by Zimmermann *et al*. [62] where they prove that that test measures fracture energy in mixed mode and not in pure mode II. These authors also analysed the ELS test in the context of bone fracture characterisation under pure mode II loading. Although this test provided accurate results, it should be referred that it has two main disadvantages when compared to the ENF. In fact, it requires a more complex testing setup and a previous determination of the longitudinal elastic modulus for each specimen.

Since the main objective of this work is to study the adhesive bond between cortical bone and bone cement, it is important to underline that only one paper was found on a mechanical test with the objective of calculating the fracture energy of the bond between these two materials. In this work [63], the authors resort to a Bilayer Compact Sandwich (BCS) test and, as such, claim to be able to determine the mode I fracture energy. About mode II tests, no articles were found with these materials and although there are no standards for testing the fracture of adhesive joints in mode II, there are tests based on the inter-laminar fracture of composites in mode II adapted for the study of adhesive joints, as is the case of ENF and ELS, for example [64].

2.2.2.1 Double Cantilever Beam (DCB)

Out of the 96 papers in the ScienceDirect [65] or PubMed [66] databases containing the words “DCB” or “Double cantilever beam” and “bone”, at the time of consultation for this literature review, only seven effectively contain DCB tests applied to bones.

The DCB test stands out due to the simplicity of its specimens' geometry and, as such, to the accessibility of the substrate manufacturing. In addition, it presents a simple execution and makes it possible to obtain the G_{Ic} value mathematically, using the Beam Theory.

Concerning the fracture characterisation of bone/cement connection, the DCB specimens are formed by two substrates glued together with a thin layer of adhesive, in which a pre-crack is introduced at one end during the manufacturing process. Throughout the test, a tensile stress is applied to both ends of the specimen arms, thus promoting a crack propagation in mode I.

Morais and his team [44] successfully applied a miniaturised version of the DCB test to cortical bone tissue. The authors considered a NLFM analysis through numerical simulation, incorporating CZMs and determined the corresponding *R*-curves. The same research team [60] used the DCB test to determine the representative cohesive laws of fracture in hydrated and dehydrated bovine cortical bone tissue to evaluate the influence of water content on cohesive laws and fracture toughness. These authors employed an inverse method based on a genetic algorithm and pointed out the changes in the ductility of the material and consequent effects in the fracture mechanisms as a function of the hydration of the cortical bone tissue.

In Table 2 are presented the G_{Ic} values found in the literature for bones tested with DCB.

Table 2 – G_{Ic} values for bovine bone measured with the DCB test

Article	Tested material	G_{Ic} (N/mm)
[44]	Bovine femur	1.91 ± 0.30
[60]	Bovine femur	1.77 ± 0.35

2.2.2.2 End-notched flexure (ENF)

The End-Notched Flexure (ENF) test consists of a three-point bending test on a specimen containing a pre-crack, which causes shear loading at the end of the crack.

Moura *et al*. [61] performed numerical analyses in order to verify the adequacy of the ENF tests to determine fracture toughness for pure mode II loading. They concluded that the specimen size should be carefully chosen to avoid erroneous measurements, due to the possibility that the central loading induces compressive stresses at the end of the crack and therefore influences the toughness measurements.

Dourado *et al*. [67] also presented the use of the ENF test. These authors performed numerical and experimental analyses considering bovine bone. The conditions of self-similar propagation were met which allowed, without any doubt, to obtain the value of the *G* for pure mode II loading from the *R*-curve. It should be noted that the authors

applied a data reduction scheme based on Timoshenko's beam theory and specimen compliance (Compliance Based Beam Method – CBBM), hence avoiding the need to monitor the crack growth during the test. The numerical analysis served to validate the procedure since it was verified that both the force-displacement curve and the *R*-curve obtained during the experimental tests are well reproduced numerically.

Silva *et al*. [68] used the ENF test to study the fracture behaviour of human cortical bone tissue under pure mode II loading. The authors validated the data through numerical analysis and digital image correlation (DIC). In this work, the force-displacement curves of the ENF test were analysed and the corresponding *R*-curves were obtained using CBBM. The DIC data allowed both to obtain the cohesive law by means of the so-called direct method and to quantify the shear deformation, i.e., the precise point on the force-displacement curve at which the initial crack starts to propagate. The authors also verified that the beginning of the crack propagation occurs after the peak load, which proves the existence of a damaged zone with a non-negligible dimension. In conclusion, the authors sustain that the ENF test is applicable for fracture characterisation of human cortical bone tissue under mode II loads.

In Table 3 are presented the G_{IIc} values found in the literature for bones tested with ENF.

Table 3 – G_{IIc} values for bovine bone measured with the ENF test

Article	Tested material	G_{Ic} (N/mm)
[67]	Bovine femur	2.25 ± 0.36
[69]	Bovine femur	2.97 ± 1.1

2.2.3 Fracture treatments

After a fracture, in most situations, the bone re-joins successfully and without major variations to its initial shape [4]; however, there may also never be a union again or there may exist a delay in this connection. Often, especially in more complex fractures, it is necessary to add a fixation system to promote a correct and faster union.

Bone fractures have existed since the existence of the human being and, as expectable, solutions and forms of treatment have always been sought. Multiple records from various eras and different places prove this. Some examples are Egyptian specimens (3 100 – 30 b.C.) found healed, which gave these people the reputation of being "skilful in treating fractures"; the reports of Al-Zahrawi (Arab surgeon, 9th century) which refer to the use of clay gum, flour and egg white to make an external splint; from this same people, but years later, the technique of pouring plaster over the injured limb is mentioned; Gersdoff (German surgeon, 16th century) describes the

use of splints made of wood held together with bandages and even the Chinese present ancient records where they mention the use of splints made with willow plates [1], [70], [71].

An inadequate fixation of the fractured zone allows movement in the site, which leads to instability. This instability compromises angiogenesis and blood vessel growth which, in their turn, complicate fracture union, thus becoming the most common cause of non-healing of the bone [4].

According to the principles of bone formation, one of the most important factors in its regeneration is the presence of blood in the recipient area [72]. Although it has been suggested that cortical perforations increase the development of blood clots and trigger the process of angiogenesis and cell migration, several studies have achieved bone regeneration without decortication [73].

Figure 14 presents different ways of treating bone fractures, with a focus on the surgical forms of treatment with internal fixators.

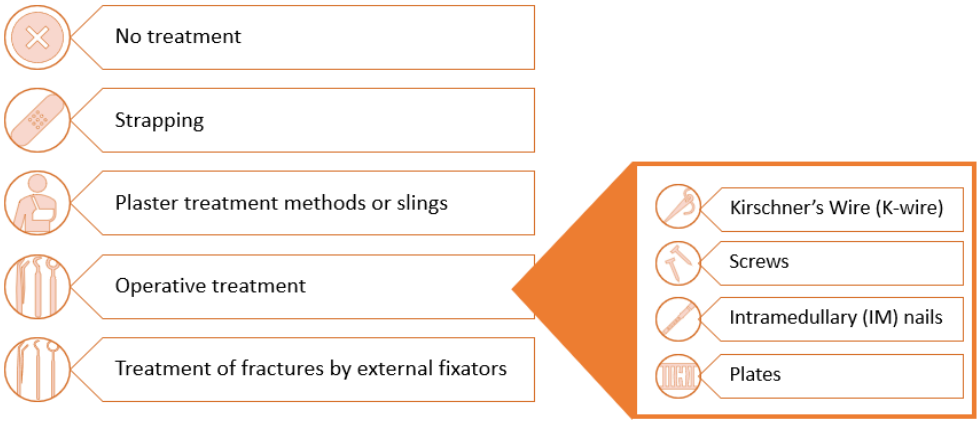

Figure 14 – Forms of bone treatment (adapted from [1], [74])

In an interview with Dr. Rosmaninho Seabra, director of the orthopaedics department at the Prelada Hospital, it was found that the most common procedure for diaphyseal fractures in Portugal is the application of osteosynthesis plates with endomodular screws or pins. As this professional mentioned that he does not usually treat traumatic problems, but more originating from fatigue, he recommended that other professionals who normally deal with traumatic fractures should be sought. Following his advice, Dr. Manuel Gutierres, orthopaedic doctor at the São João Hospital Centre and professor in various curricular units at the Faculty of Medicine of Porto University, among which the "Traumatology" unit, was also interviewed. This professional reinforced what was said by the first one, but also stating that, in orthopaedics, few evolutions have occurred in the last few years and that there is a need for engineers to ally with medics in the search for new solutions, ideally less evasive.

2.2.4 Bone cement

When a bone is fractured, it is imperative to maintain its alignment during the recovery phase in order to ensure its correct healing. In situations where it is not possible to maintain alignment in the face of external fixators (such as plaster, for example), it is compulsory to apply internal fixators; however, conventional internal fixation methods are associated with several clinical problems [75]. As such, the use of another form of fixation, ideally non-metallic and in the form of an adhesive, could be a colossal asset to aid fracture repair.

For this reason, several types of adhesives have been tested in an attempt to bond bones:

- The epoxy group shows promising properties, but since they are not biocompatible, they develop adverse reactions in living beings and therefore cannot be used. Moreover, in humid environments their mechanical properties are greatly sacrificed [76];
- Polyurethanes also exhibit poor mechanical properties in wet media. Episodes of bone disturbance, infection or even necrosis have also been reported [76]. Nevertheless, this group of materials has shown very good performance in recent studies, as was the case of a polyurethane foam reinforced with hydroxyapatite crystals successfully developed to bond bones together [77];
- Methacrylates and cyanoacrylates belong to the class of adhesives that are considered to have a high potential for adhesion to bones [78].

DIN EN 923: 2016-03 standard [79] defines an adhesive as a non-metallic substance capable of joining materials by surface adhesion and internal strength (cohesion). This same standard considers bone cement to be an adhesive. Nonetheless, despite the definition in the standard and its wide use, whether due to the lack of adhesive properties, local stresses in the adhesive region or unsuitability of bone cement for delicate fractures, the suitability of bone cement as a bone adhesive is a matter of debate. In the literature, different approaches have been presented in order to overcome these barriers [80].

Polymethylmethacrylate (PMMA) is the main constituent of the most widely used bone cement nowadays [81]. This material is widely used in the fixation of implants in orthopaedic and traumatic surgeries, in the fixation of pathological fractures and in the repair of bone defects [82], [83].

Calcium phosphate cements (CPCs) and glass polyalkylene cements are commercial alternatives to PMMA. These options are successfully used in orthopaedic and dental applications; however, although CPCs are bioabsorbable and biocompatible, they are only used in cranial and maxillofacial surgery due to their low mechanical strength [84].

The polymerisation process (elaboration of the bone cement) lasts between seven and fifteen minutes and contemplates four phases [81]. These phases, as well as a brief description of each one, are described in Figure 15.

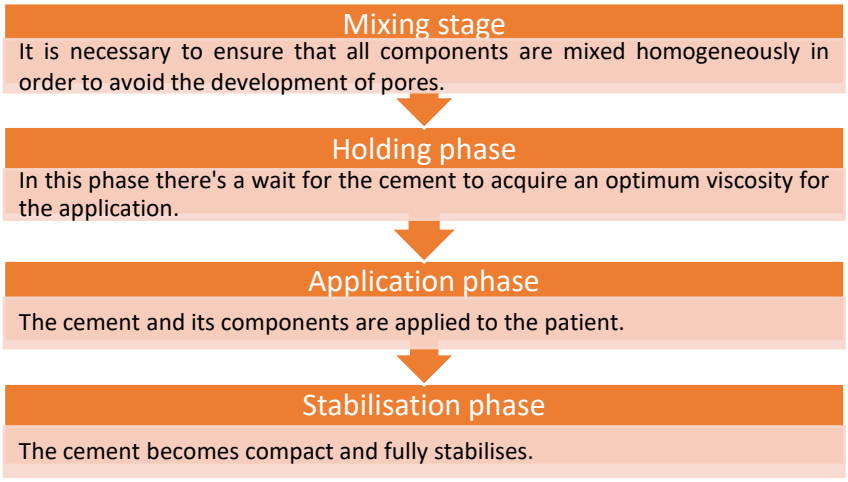

Figure 15 – Bone cement polymerisation process (adapted from [81])

It should be emphasised that some authors argue that the term “cement” is not very adequate, as it is usually used to describe a substance that joins two objects, and this is not the case here. This material does not possess adhesive properties and only acts in the filling of areas, creating a tight space between an implant and the bone, where it acts as if it were a “grout” [82]. Even though, the term cement was adopted along this dissertation.

2.3 Application of finite element analysis to bone fracture

There are common engineering problems that can be translated by differential equations. The finite element method (FEM) is a way to solve these problems by means of approximate solutions (numerical solutions). In other words, they resort to simple approximations of unknown variables and transform partial differential equations into algebraic solutions [85]. In the FEM, the geometry of the structure to be analysed is first reconstructed and then exported for pre-processing, where it is divided into small elements of simple geometric shape connected by specific points, the nodes, defined by coordinates. In these nodes, the existence of degrees of freedom is considered, being compatibility and equilibrium conditions imposed on them. The elements are mathematical expressions obtained from the degrees of freedom of the nodes, which describe the displacements inside the element. Only in the common nodes there is a passage of information between different elements and the set of elements that constitute a structure is called a mesh.

Figure 16 presents an illustrative scheme of the FEM for a better understanding of this concept.

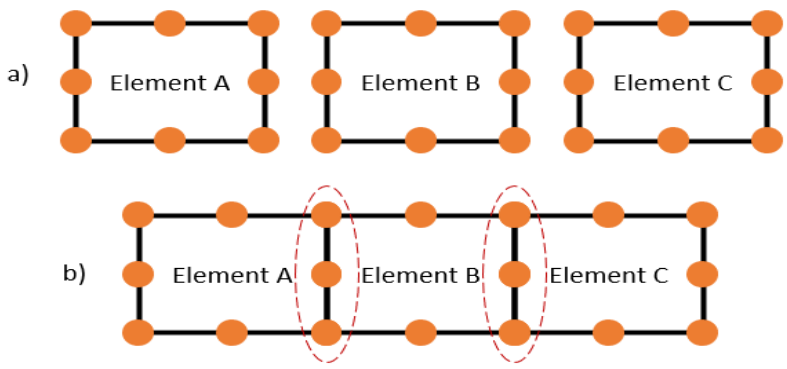

Figure 16 – FEM illustrative scheme (adapted from [3])
The orange circles correspond to nodes and the dotted area marks the nodes shared between elements. In the upper part of the image [a)] there is no transmission of information between the elements. On the other hand, in the inferior part [b)], once there is a sharing of nodes, the information is transmitted between the neighbouring elements.

The use of this technique in a biomedical context is particularly useful because it reduces animal experimentation, which is always a controversial and expensive subject, but also because it enables a greater range of simulations and consequent predictions of the structure's behaviour. In the context of the present work, this technique is intended to compare and confirm data obtained experimentally.

As previously mentioned, bone tissue can be seen as a quasi-fragile material characterised by a non-negligible FPZ since, during a fracture, several inelastic and dissipative processes occur in the region in front of the crack's end. These are responsible for a not negligible dissipation of energy, which makes the application of LEFM concepts unfeasible. Consequently, NLFM approaches are more appropriate, and CZMs are particularly suitable to deal with fractures of quasi-fragile materials, as is the case of the bone. The application of CZM to fracture behaviour of cortical bones has been referenced by some authors ([38], [86]–[88]). These models integrated with the finite element analysis show great potential, as they allow the influence of several factors to control the fracture initiation and damage propagation to be analysed.

An alternative approach to CZM is the extended finite element method (X-FEM), which has also been applied by some authors [50], [89], [90]. Both approaches have advantages in the simulation of crack initiation and propagation, such as the fact that they require a lower computational cost compared to other finite element techniques with the same level of accuracy. In spite of this, they also have limitations, such as the fact that a predefined crack path is required in the case of CZM, or the lack of crack multiplication and bifurcation in X-FEM-based models [91].

DEVELOPMENT

3.1 Experimental component

3.2 Numerical component

3.3 Results

3.4 Discussion of results

3 DEVELOPMENT

Biological materials have low resistance to fracture, reason why they usually fail. As a result, it becomes particularly useful to understand the characteristics of these materials, and to use the knowledge that has been developed for engineering materials in order to apply it to the study of the biological materials failure, as is the case of the bone [27]. Accordingly, in this chapter, the knowledge of FM is applied to characterise the adhesive bond between bone and bone cement.

3.1 Experimental component

This subchapter presents all the steps of the experimental work performed. Here, the used materials, equipment and accessories are described, as well as the steps for the specimens' manufacturing and mechanical tests' parameters.

3.1.1 Materials and equipment

With the aim of studying the connection between bone cement and bovine femurs, there is a need for these two materials and some more equipment which allow the chosen tests to be carried out. Therefore, in this subchapter, the materials and equipment used will be presented and described.

3.1.1.1 Bone

As previously mentioned in the second chapter, bone can present different shape types and, according to the respective type, it can have a greater or lesser quantity of each one of the main categories of tissues (cortical and cancellous). Each of these categories presents distinct characteristics and, therefore, it is necessary to study them separately as two different materials. The objective of the work is to study the structural constituent that will be linked to the structure developed by the project where this dissertation is concerned. For that, the specimens of the present dissertation were elaborated with cortical bone of bovine femurs, acquired in butcher shops partners of the project, so because of that without any controlled conditions like age.

Long bones usually possess a certain curvature. This curvature is fundamental to absorb the tension of the body weight in several points, thus allowing a more uniform

distribution [5]. Nonetheless, due to this curvature, obtaining specimens for testing becomes quite complicated. In addition, the classical fracture tests used for other materials require special adaptations due to the characteristics of the bone [40], thus, given the anatomical curvature of the femurs (with an example visible in Figure 17), only the bone regions corresponding to the medial region were used. It is important to outline that, in order to keep the properties of the bone as similar as possible among different specimens, the proximal and distal region along the sagittal plane of the femur were used.

Figure 17 – Example of a bone part

3.1.1.2 Bone cement

With the purpose of using a material that adheres to bone, a literature search was carried out, from which it was found that a bone adhesive that meets all the requirements to be applied in the treatment of bone fractures has not yet been identified [76], [92]. Epoxy adhesives cannot be used, because they are not biocompatible and those with better properties in the bone are the methacrylates and cyanoacrylates.

As already mentioned, the DIN EN 923: 2016-03 standard [79] defines an adhesive as a non-metallic substance that is capable of joining materials by surface adhesion and internal strength (cohesion), and considers bone cement as an adhesive. Although multiple sources report that PMMA-based bone cements only bond to tissues by mechanical adhesion (anchorage), without exhibiting adhesive properties, the bonding chosen for this project to characterise was PMMA-based, as it is one of the most commonly used bone cements nowadays. This way, the DePuy CMW 3 bone cement from DePuy Synthes was used (Figure 18), being its components depicted in Figure 19.

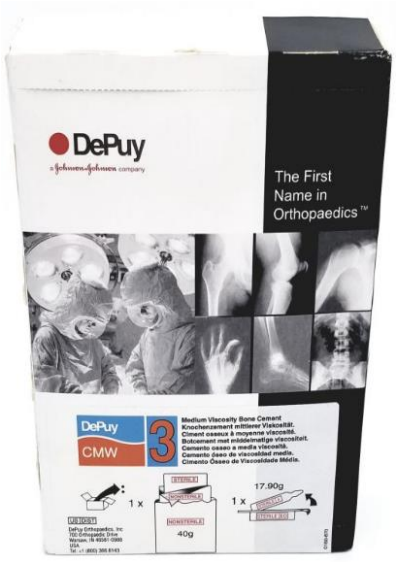

Figure 18 – Bone cement chosen

Figure 19 – Components of the bone cement chosen

This is a medium viscosity cement which, inside the box (Figure 18), contains two packages: a bag with powder and a flask with a liquid (Figure 19). These two items must be mixed together in order to obtain the final substance. The powder is a mixture consisting of 97% Methyl methacrylate and 3% N-Dimethyl-p-toluidine. The liquid is the reagent.

It should be noted that, according to the manufacturer himself, this cement has a handling time as shown in Figure 20. For example, for an environment temperature of approximately 19 °C, one can only handle the cement up to 11.5 minutes after mixing the substances and, after 12.5 minutes the compound is already hardened. This means that there is little time to apply the cement to the bone.

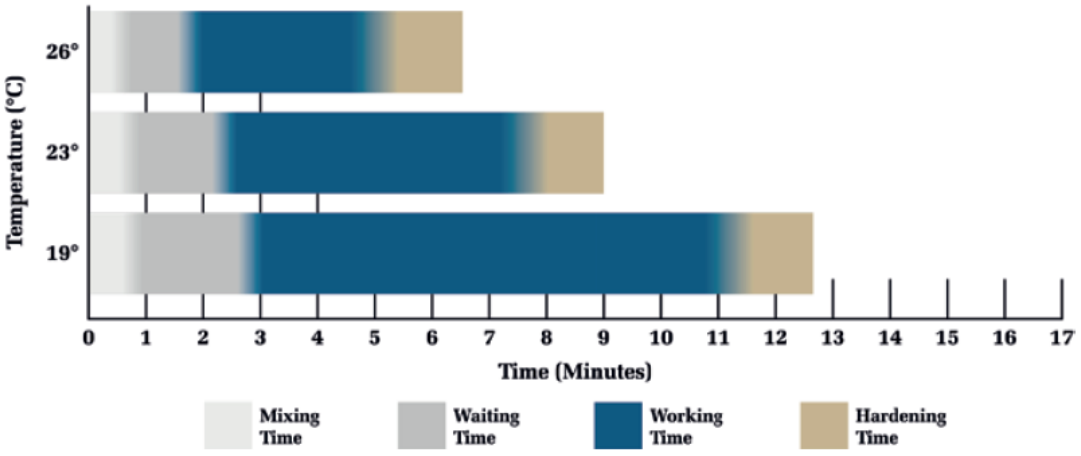

Figure 20 – Cement working time [93]

The mechanical properties of DePuy CMW 3 cement are shown in Table 4.

Table 4 – Mechanical properties of DePuy CMW 3 cement (adapted from [93])

Property	Productor Value [MPa]	Minimum Standard ISO 5833:2002 [MPa]
Compressive Strength	110	70
Flexural Strength	75	50

3.1.1.3 Equipment and accessories

The equipment and accessories used were essentially intended for two main tasks: the manufacture of specimens and the mechanical tests to carry out.

For the specimens' manufacturing:

- Manual bow saw with SANDFLEX Bi-metal + Cobalt blades [94];
- Gambin 11M milling machine (Figure 21) with a Sandvik R216.34-16050-AK32H 1620 end mill (Figure 22)[95].

Figure 21 – Milling machine used setup

Figure 22 – Highlight of the milling tool used

For the mechanical tests:

- Equipment designed by the University of Minho and Faculty of Engineering, University of Porto with accessories designed for this purpose (Figure 23).

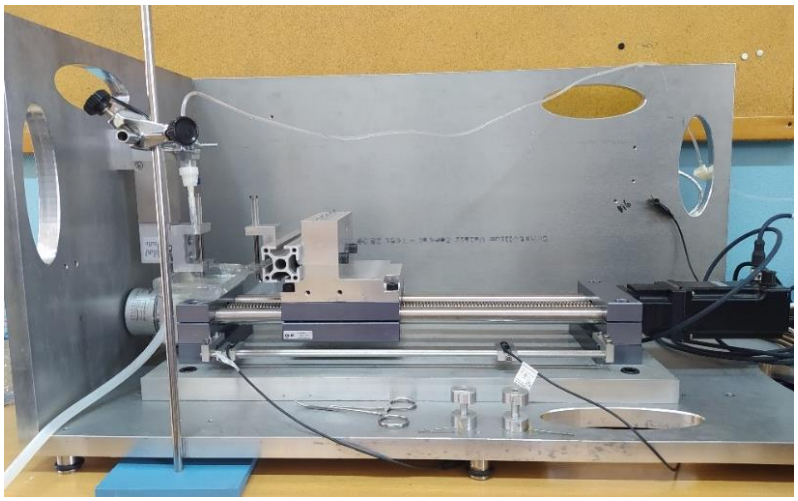

Figure 23 – Equipment used for mechanical tests with the accessories for the DCB tests

- Instron 8801 fatigue testing machine [96] from the University of Trás-os-Montes and Alto Douro (Figure 24).

Figure 24 – Testing machine

- HAAS VF2 machining centre for the manufacture of some accessories (Figure 25).

Figure 25 – HAAS VF2 machining centre

3.1.2 Experimental sequence

The experimental component of the present dissertation is essentially divided into two parts. The first one consists in the manufacturing of the specimens and the second one involves mechanical testing. In the next subchapters these two steps will be presented and explained in detail.

As mentioned before, this dissertation is focused on long bones and, more specifically, on bovine femurs. As expected, right after the extraction of the bones from the animal, these materials have large dimensions, an irregular surface and more than one type of tissue. Thus, before carrying out the tests, it is necessary to reduce its dimensions, bring the shape closer to that defined by the mechanical tests and remove all tissues that are not the object of study (cortical bone). In resume, from the raw material to the final shape of the specimens several production steps are required.

The stages undergone for the manufacturing of the specimens can be split into four main categories: cutting, cleaning and conservation, sizing, and gluing. A deepening of the stages with their sub-steps can be observed in Figure 26 and then a more detailed discussion is presented forward.

Figure 26 – Stages for the specimen' manufacturing processes

The first two cuts, performed with a butcher's cutter, consisted of the removal of the proximal and distal epiphysis. After this step, a piece similar to the one presented in

Figure 27 was obtained. Afterwards, a longitudinal cut (Figure 28 and Figure 29) had to be made in order to divide the diaphysis into two parts, i.e., the internal and the external one (Figure 30).

Figure 27 – Bone piece without the epiphyses

Figure 28 – Step of cutting longitudinally the diaphysis

Figure 29 – Longitudinal sectional cut of the bone

Figure 30 – Complete longitudinal cut of the bone

As this is a biological material, cleaning and conservation become matters of the utmost importance. Thus, after the opening (Figure 30), all the materials which may rot and cause bad odours are removed, i.e., veins, blood, marrow, and flesh. Figure 31 and Figure 32 show images of the cleaning stage.

Figure 31 – Marrow removal

Figure 32 – Bone after some cleaning

Since the bone pieces had a certain curvature and the goal was to make parallelepiped-shaped specimens, the next step consisted of facing operations. For these operations, a milling machine with a helicoidal cutter was used, which was prepared to work at a speed of 1120 rotations per minute. The choice for this speed was due to the trial-error method in which low speeds increased the propagation of cracks, causing chipping, and very high speeds caused a greater heating in the cutting region (even though it was hydrated), that apparently led to a kind of melting of the material, clearly changing the surface geometry.

The machine was programmed for the option of moving the table manually, in order to allow a greater control of the movement and operations. It was taken in account that the rotation movement of the cutter was always on the outside of the specimen so as not to cause chipping and it was never removed more than 1 mm at a time in the Z-axis. Figure 33 shows the facing operations.

Figure 33 – Bone facing operations

Both faces being flat, it was time to get the right dimensions. With the help of a set square, calliper and pen, the right dimensions were marked according to the type of test that was going to be performed. Then, again with the milling machine and with the help of the clamping press (Figure 34), the dimensions were rectified, resulting in parallelepiped-shaped bone pieces, the future arms of the specimens.

Figure 34 – Bone piece in the clamping press

The next step was the manufacturing of glued joints between two bone pieces and the bone cement. Taking into account the manufacturer's indications and a failed first attempt, due to the setting time not exceeding 10 minutes, the cement was divided into four equal parts before the reaction, so there may be slightly more than half an hour of operation in total. For this, help was requested from the chemical engineering department. A volumetric pipette, compressed nitrogen and several flasks were used (Figure 35), allowing to equally separate the monomer from the flask with the liquid component, and a precision balance was used to separate the powder component (Figure 36).

Figure 35 – Separation of the liquid component from the bone cement

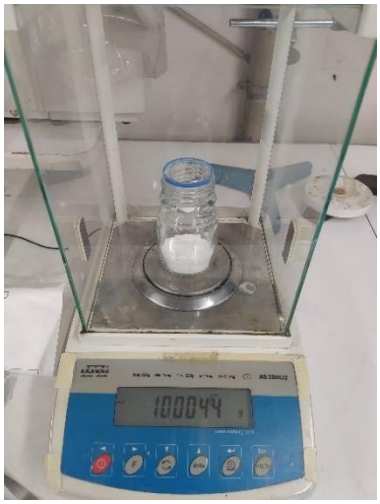

Figure 36 – Separation of the solid component from the bone cement

After this separation, gluing procedures were performed. Due to the pasty texture of the adhesive, a piece was placed on one of the specimen's arms, an attempt was made to spread it quickly and then the other arm was placed on its top, pressing them against each other, so that the adhesive excess could be removed. The specimens were obtained from the same sample and aligned with the help of accessories, and at the end of the curing process, these specimens were obtained as shown in Figure 37. As it is clearly visible in this figure, there is an excess of adhesive on the edges of the arms and, as this influences the strength of the specimen, it was necessary to remove it. This removal was performed as carefully as possible with 240 grit wood sandpaper. Figure 38 shows the removal of adhesive excess. After this process, the specimens were ready to be tested.

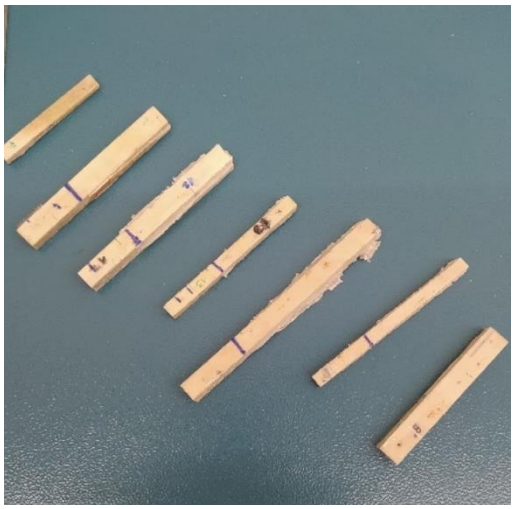

Figure 37 – Specimens after gluing

Figure 38 – Sanding step

As the manufacturing process is very time-consuming, before gluing them was often necessary to preserve the bone pieces overnight. Thus, in an attempt of trying to keep the bone as close as possible to the real conditions, the emphasis was on hydration. For that, the bone was sprayed multiple times with oxygenated water during the day and kept wrapped in saline solution-soaked gauze during the night, being frozen at a temperature of -5 °C.

There are articles reporting a significant difference between the properties of a hydrated and a dehydrated bone [49]. For this reason, during the manufacture of specimens, it is always tried to keep the bone hydrated; however, the saline solution reacts with the bone cement, ending up degrading it in a short time. As such, in this first phase, after applying the cement, the bones were never hydrated. In the future, another solution that better simulates the internal environment of the human body will be pursued and the tests repeated, but with specimens that are always hydrated.

3.1.2.1 Experimental tests

There are several mechanical tests used with both bones and glued joints. In this report, there is an attempt to perform a first fracture characterisation between two

different materials on which very little published information exists. For this reason, characterisation in the two main pure loading modes is performed using tests that were considered the most advantageous for them.

3.1.2.1.1 DCB tests

A major advantage of the DCB testing is the fact that it provides stable growth with a long fracture process zone, which allows a self-similar propagation and avoids spurious effects influencing fracture energy measurements.

The specimens destined for the DCB tests have a geometry as depicted in Figure 39. This same figure presents a caption with the most used nomenclature to describe the dimensions of this test, which are also used throughout the dissertation.

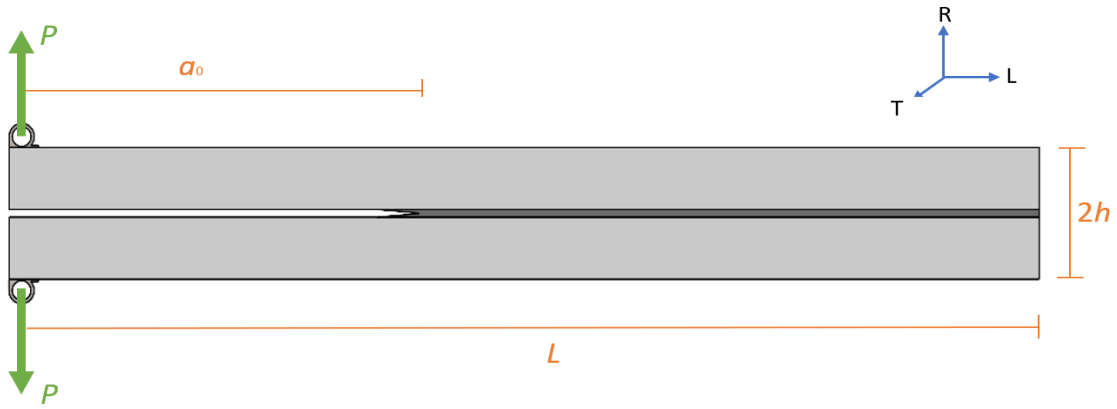

Figure 39 – Geometry of the DCB specimens with width *B*

Figure 40 represents a real specimen ready for testing. In this image, it is clearly noticeable the distinction between the different constituents of the specimen: two arms made of bone, a thin layer of cement with negligible thickness and two metallic applications, glued to the bone with Araldite® 2015, fundamental for its fixation in the testing machine.

Figure 40 – Specimen for the DCB test

It is important to highlight the difficulties that were faced until this final geometry was obtained. The standard for DCB tests requires the drilling of two holes equidistant from the centre and aligned between themselves, in each of the specimen's arms;

however, this was not feasible due to the small dimensions of the arms. A second attempt was to apply small pieces of bone (with similar dimensions to the metal pieces of Figure 40) at the end of each arm with a central hole; yet, due to their high depth, reduced length and width, and the vibration of the machine itself when drilling, it was not possible to guarantee a hole always central along the whole depth. The next solution was the one presented in Figure 40, considering small metallic pieces with a hole that allows the fixation.

The fact that there are, in reality, two types of joints glued to the specimen, does not represent a problem. In fact, the theoretical resistance supported by the Araldite® 2015 adhesive is several times higher than that supported by the bone cement and, as such, the load that is applied has no effect on the region glued with Araldite® and is totally transmitted to the specimen arms. This way, such a clearly rigid connection is obtained that, at the end of each test, it was confirmed not to have yielded, so there is no suspicion that the displacement which appears in the test is influenced by this factor.

Due to the different initial geometry, manufacturing time, complexity of working this material and not knowing what the ideal dimensions for the test are, the produced specimens do not possess the exact same dimensions. Therefore, Table 5 shows the dimensions of each specimen used in this test.

Table 5 – Dimensions of the DCB tests specimens

Specimen	a_0 (mm)	L (mm)	$2h$ (mm)	B (mm)
3	30.0	90.9	7.8	8.1
6	30.0	92.3	7.6	6.2
7	30.0	94.3	7.0	9.6
9	30.0	78.3	9.0	11.0
12	30.0	92.6	9.4	10.0
13	30.0	81.6	7.2	7.4
14	30.0	60.3	5.6	6.75

Note: All specimens were made and numbered sequentially. Then, according to their morphological characteristics, it was decided which ones would be used in fracture, which would be used for fatigue (dissertation by the student Teresa Campos) and which would go to the DCB or ENF tests. Hence, this is why the numbering in the table is not sequential.

Each parameter in Table 5 was obtained from what each bone allowed. The only parameter that was chosen and defined was a_0, parameter that was defined so that the ratio h/a_0 was acceptable by the Timoshenko's beam theory.

After all dimensions were recorded, the tests began. One by one, each specimen was mounted with a setup equal to the one presented in Figure 41. In this fracture test, one of the arms is fixed and a displacement is applied to the other, thus causing two symmetric loads, P, applied at the ends of each of the specimen's arms. Accordingly, this loading force crack growth under pure mode I loading.

Figure 41 – Setup for the DCB test

Through a program developed in Arduino and connected to the testing equipment, the test was initiated. The equipment was programmed to apply a displacement rate of 0.1 mm/min, giving rise to a very slow displacement and allowing a gradual crack propagation. In the course of the test, the software registered the respective load and displacement value for each instant. The data were all exported to an Excel file for post-processing analysis.

3.1.2.1.2 ENF test

The ENF is a three-point bending test with two glued beams of equal dimensions, except in the region of the pre-crack. The load causes a shear stress in the adhesive, thus allowing to obtain the *G* under pure mode II. The specimens used in this testing group have a geometry as shown in Figure 42. This figure presents a legend with the nomenclature which is the most used to describe the dimensions of this test and will be adopted throughout this report.

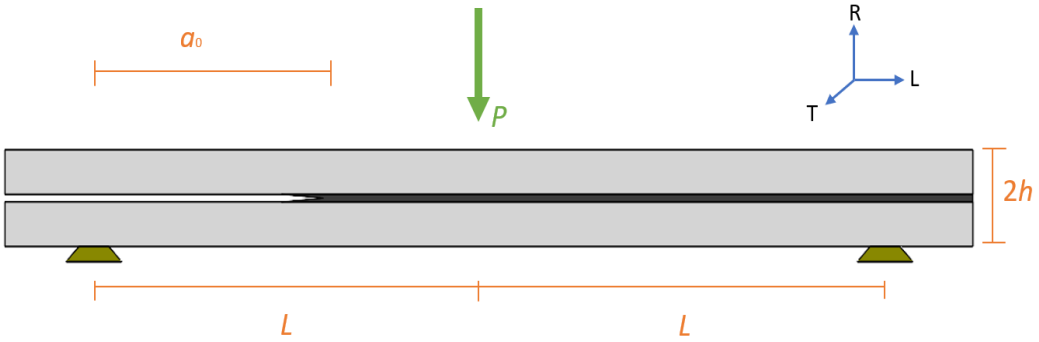

Figure 42 – Geometry of ENF specimens

Figure 43 shows a real specimen used in this testing group. This image clearly shows the distinction between the different components of the specimen, two bone arms of equal dimensions and a thin layer of cement joining them.

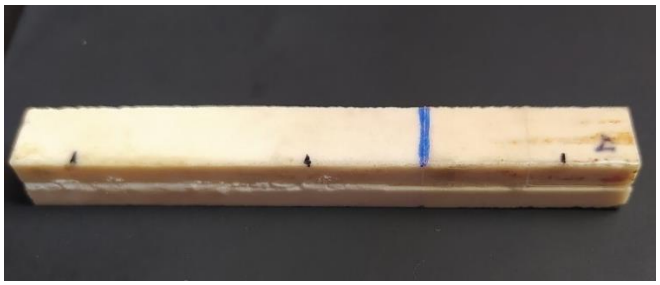

Figure 43 – ENF test specimen

Once again, and for the same reasons as the DCB test, the dimensions of the different specimens are not the same. Table 6 shows the dimensions of all specimens destined for the ENF fracture test.

Table 6 – Dimensions of the ENF test specimens

Specimen	a_0 (mm)	2L (mm)	2h (mm)	B (mm)
1	22.7	90	8.2	9.4
4	10.2	75	9.4	6.9
5	17.7	75	6.8	9.6
6	25.0	85	7.6	6.2
8	21.9	90	8.4	9.5
10	23.1	90	7.6	9.1
11	25.0	85	7.2	11.5
15	21.9	100	7.8	9.7

After every dimension registered, the tests began. One by one, each specimen was assembled with a setup similar to the one shown in Figure 44.

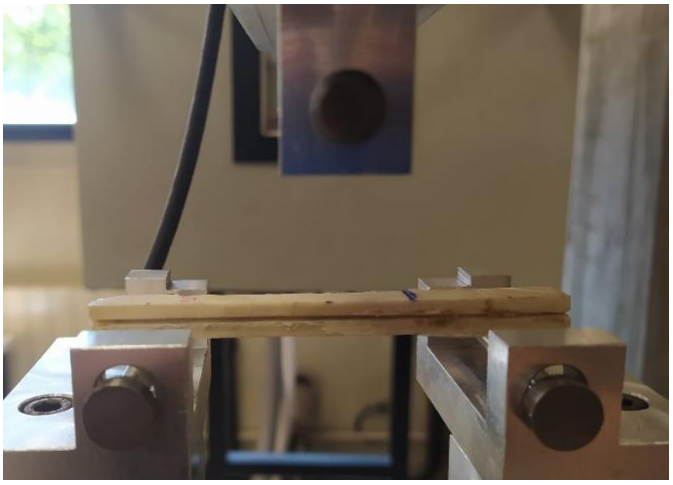

Figure 44 – Setup for the ENF test

The equipment was programmed to apply a velocity of 0.3 mm/min in order to induce a gradual crack propagation. During the test, the software registers the respective value of the load and displacement for each instant.

The first tested specimen fractured in the central region, which indicates that the bone resistance was overcome, but the connection resistance was not reached. To

overcome this, it was tried to reduce the bonding section and make a V cut on each side of the specimen in the bonding region. Therefore, in addition to reducing the bonding section, a concentration of stresses was induced foreseeing to compel crack growth at the specimen mid-plane. Figure 45 shows the tearing process on the sides of the specimen.

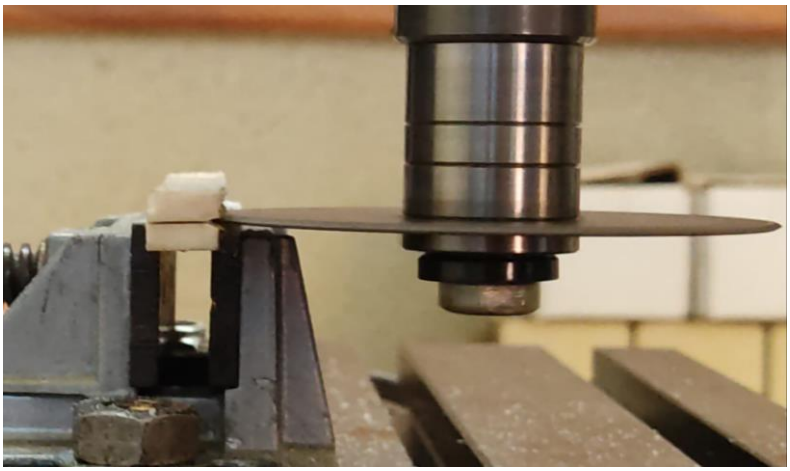

Figure 45 – Tearing process on the sides of the specimen

The second test specimen, already with the V-shaped grooves, fractured again in the central region.

A third, successful attempt was to increase the distance between supports (2*L*), thus diminishing the flexural stiffness of the specimen. Vertical black lines (Figure 46) were marked on the lateral surface of the specimen for a better visual perception of a misalignment between the specimen arms during the test, revealing the presence of a shear loading.

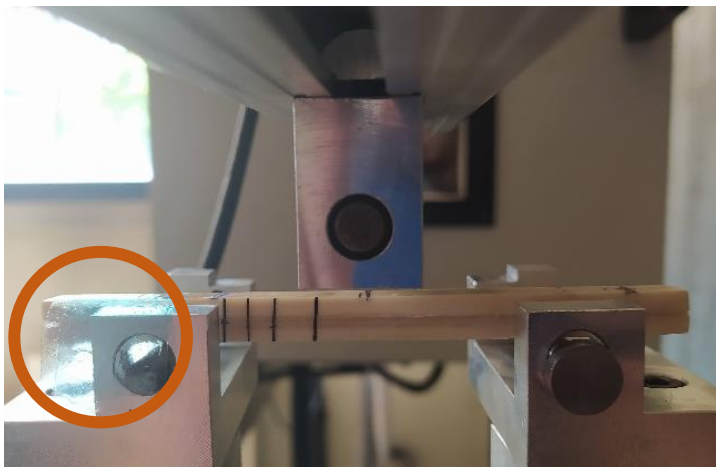

Figure 46 – Traces made on specimens to perceive the existence of shear during the ENF test

Also in Figure 46, it is possible to verify the existence of a piece of blue Teflon® film on the left side of the specimen (within the brownish circle) to create the pre-crack region. The Teflon film was embedded with an oil (purified Vaseline, in this case),

aiming to minimise the friction between the specimen arms during the test that will lead to spurious increase of fracture energy under mode II loading.

After these tests, the data were exported to Microsoft Excel® for post-processing purposes.

3.2 Numerical component

In this project, there were two types of numerical simulations. The first one was to estimate the Young's Modulus for each of the specimens and the second to validate the experimental procedure. Both approaches were carried out using the Abaqus® software.

3.2.1 Estimate the Young's Modulus

As already mentioned, the bone is a natural and consequently heterogeneous material with a large scatter on its elastic properties, so it was necessary to estimate the value of the Young's Modulus for each specimen. For that, a two-dimensional finite element routine with 3378 eight-node plane stress elements (CPS8) and 1080 six-node cohesive elements located in the central zone was used for DCB specimens. The value of the Young's Modulus of each specimen was obtained when the slope of the numerical *P-δ* curve was approximately equal to the experimental one.

3.2.2 Validation of procedure

As previously mentioned in the literature review, bone cement can be seen as a brittle material and bone tissue as a quasi-brittle material characterised by a non-negligible FPZ (in front of the crack's end). In this region, several inelastic and dissipative processes occur during the fracture formation, leading to the dissipation of a relevant amount of energy, which makes the application of the LEFM concepts unfeasible; therefore, one must resort to NLFM approaches. Accordingly, CZMs become particularly interesting, because they can be applied to quasi-brittle materials and are able to account for the energy dissipated in the non-negligible FPZ.

Ural *et al* [97], in 2006, performed a finite element analysis to reproduce the experimental *R*-curve behaviour in cortical bone specimens with the CT test. These authors used cohesive elements along the crack path and concluded that this approach predicted the experimental results. Morais *et al* [44] and Pereira *et al* [60] used, as well, finite element methods with a cohesive law, but applied to the DCB test. These two works identified the cohesive law parameters based on a trial-error process, fitting the numerical curve with those obtained experimentally. The same process, but applied in mode II, was presented by Pereira *et al* [40] and Dourado *et al* [67].

Following what was mentioned in the literature, numerical analyses with cohesive zone modelling of the DCB and ENF fracture tests (Figure 47) were performed with the aim to validate the experimental procedures, which were applied in order to estimate

the fracture energies in pure modes (I and II). For the DCB test (Figure 47 [A]), it was used the same finite element routine as to estimate the Young's Modulus. On the other hand, for the ENF test (Figure 47 [B]), a routine with 2538 eight-node plane stress elements and 810 six-node cohesive elements was also used in the crack propagation zone. In the simulations for each type of test, average dimensions and fracture properties were used. In addition, small increments were considered in order to ensure a smooth propagation of the damage zone.

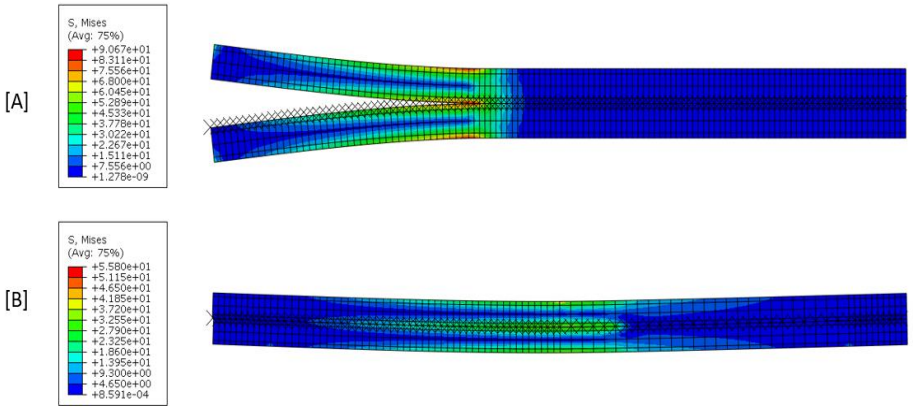

Figure 47 – Meshes and profile of the von Mises stresses obtained for an example specimen of each test type used. [A] corresponds to specimen 13 and is an example of the DCB test. [B] corresponds to specimen 15 and is an example of the ENF test

In the work of Pereira *et al* [40], the authors employ the concept of equivalent crack to determine the values of G_{IIc} and propose the application of a linear cohesive law to validate the results. Due to the small fracture energies obtained in the experimental component, it was considered that the simplest linear softening cohesive law (Figure 48) would also be adequate to validate the tests performed in the scope of this dissertation. This law requires the σ (local stress) and the respective G (energy release rate, which corresponds to the triangle area), being the δ (displacement) calculated as a function of the maximum local stress and the stiffness at the interface. The value of the initial stiffness is defined as the highest value that does not induce numerical problems and, according to Moura *et al* [98], most structural problems are solved with a number between 10^6 and 10^8 N/m^3. So, the corresponding cohesive parameters are listed in Table 7 and the value of 10^6 were used for initial stiffness.

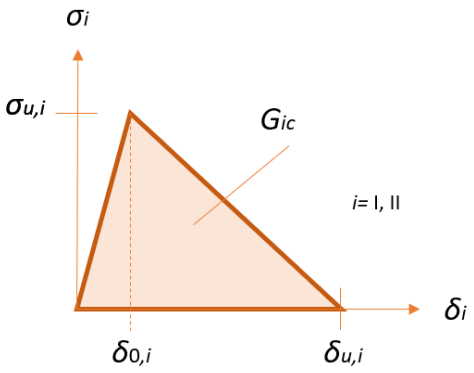

Figure 48 – Triangular softening law used

Table 7 – Cohesive parameters used

Mode I		Mode II	
σ_u [MPa]	G_{IC} [N/mm]	τ_u[MPa]	G_{IIC} [N/mm]
10	0.074	10	0.059

3.3 Results

The data extracted directly from the used testing equipment require a certain post-processing, in order to obtain the energy release rate values in each loading mode, which is the main objective of this dissertation. Hence, in this subchapter, the raw results obtained will be presented and the post-processing method explained until the final results are achieved.

3.3.1 DCB test

Out of the seven specimens intended for this test, one of them fractured in a region other than the union between the bone and the adhesive, and a second one does not show evidence of crack propagation by the cement; therefore, only five specimens presented valid results that will be considered. All tests were performed without hydration and during the fracture tests the applied displacement and the respective load were continuously registered.

The graph in Figure 49 shows the *P-δ* curves (force vs. displacement) for the valid DCB tests, directly after the extraction of the data from the machine, with minimal processing. This figure also shows a numerical simulation which was performed.

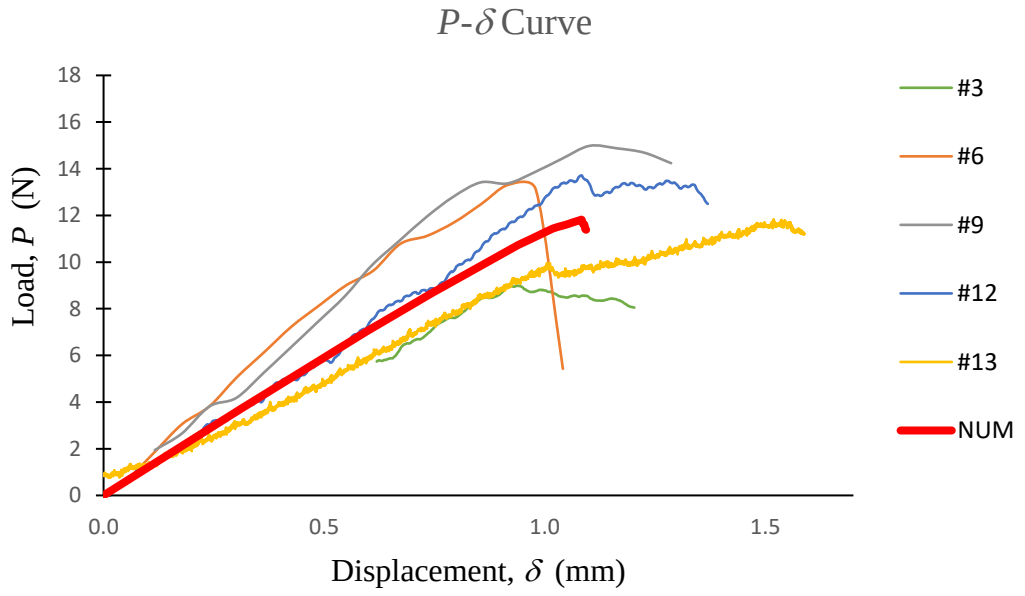

Figure 49 – *P-δ* curves of the DCB tests

The compliance, C, of the specimens can be calculated by equation (1), i.e., by the ratio between displacement and load. Thus, considering only the initial slope of the curve in Figure 49, it is possible to obtain the stiffness values (inverse of the compliance) for all the DCB specimens in Figure 50.

$$C = \frac{\delta}{P} \tag{1}$$

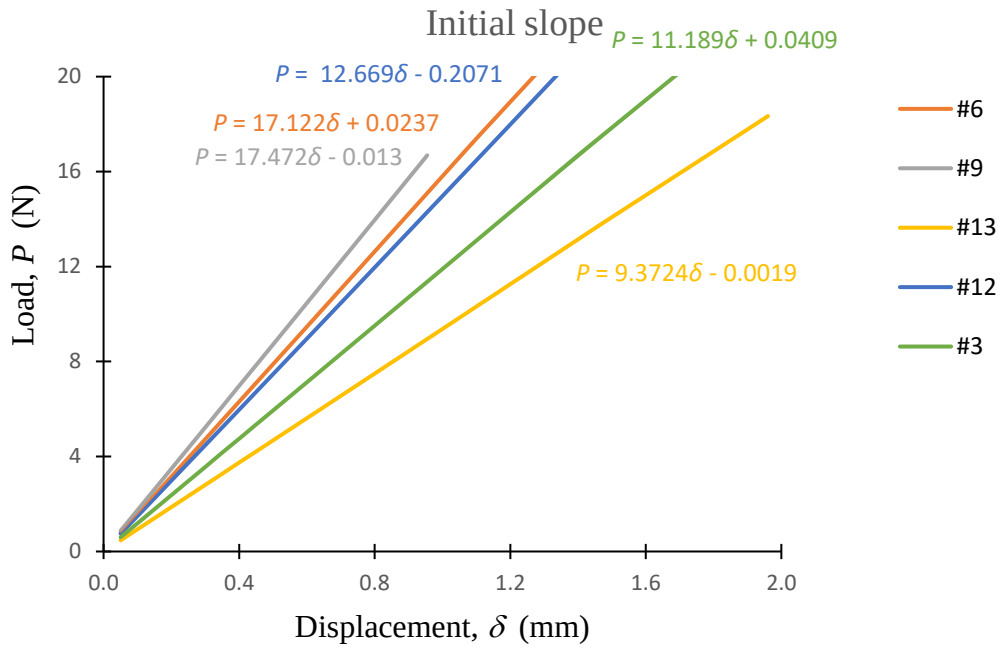

Figure 50 – Values for the specimens' stiffness, for the DCB test

The calculation of this slope is of particular importance, since it allows the correction of the displacement values obtained experimentally, and thus to reduce measurement errors.

The specimen compliance is registered in the course of the fracture test and is subsequently used to estimate the equivalent crack length. With this aim, the following equation (2) based on Timoshenko's beam theory, establishing a relation between the specimen compliance and the crack length, can be employed [99].

$$C = \frac{8a^3}{E_L B h^3} + \frac{12a}{5BhG_{LR}} \tag{2}$$

where E_L is the longitudinal modulus of elasticity, G_{LR} the shear modulus in the LT plane, B and h are dimensions of the specimen and a is the crack length (Figure 39). The equivalent crack length, a_e, during a fracture test can be obtained from the current specimen compliance [100], considering equation (3), i.e.,

$$a_e = f(C) \tag{3}$$

The solution of the cubic equation (4) can be obtained using the Matlab software [96].

$$a_e = \frac{1}{6\alpha} A - \frac{2\beta}{A} \tag{4}$$

where

$$\alpha = \frac{8}{Bh^3 E_L} \; ; \; \beta = \frac{12}{5BhG_{LR}} \; ; \; A = \left(\left(-108\gamma + 12\sqrt{3\left(\frac{4\beta^3 + 27\gamma^2\alpha}{\alpha}\right)}\right)\alpha^2 \right)^{\frac{1}{3}} \tag{5}$$

being γ = - C. Therefore, combining the Irwin-Kies equation (6),

$$G_I = \frac{P^2}{2B} \frac{dC}{da_e} \tag{6}$$

where P is the applied load. With equation (2), the $G_I = f(a_e)$ relationship (i.e., the R-curve) is obtained (equation (7)):

$$G_I = \frac{6P^2}{B^2 h^3} \left(\frac{2{a_e}^2}{E_L} + \frac{h^2}{5G_{LR}} \right) \tag{7}$$

Considering the fact that the bone is a natural and heterogeneous material with inherent remarkable variability of its elastic properties, the value of E_L was estimated for each specimen by an inverse procedure. For this, with the actual dimensions of each specimen (B, h and a_0) and with multiple iterations of numerical simulations in the Abaqus® software [101], the value of the initial numerical stiffness was adjusted, by changing the longitudinal elastic modulus E_L, until it has corresponded to the experimental stiffness.

By plotting a graph between G_I and a_e, it is possible to determine the value of G_{Ic}, which corresponds to a plateau that follows the initial rising trend. This plateau is representative of self-similar crack growth conditions and defines the critical fracture energy under mode I loading (to Figure 56).

With the main goal of showing the variance of the obtained R-curves, Figure 57 presents every R-curve regarding the DCB test.

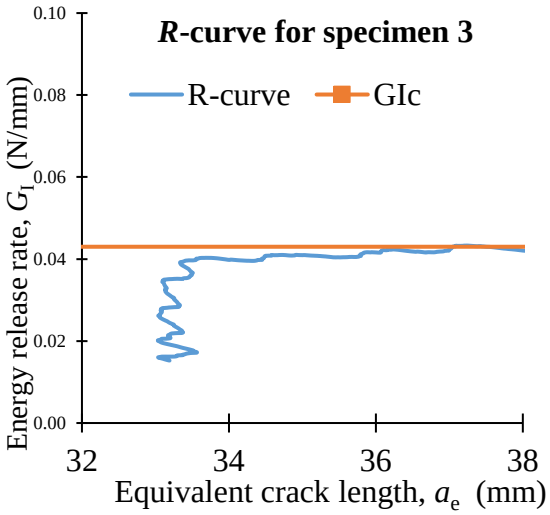

Figure 51 - *R*-curve for specimen 3

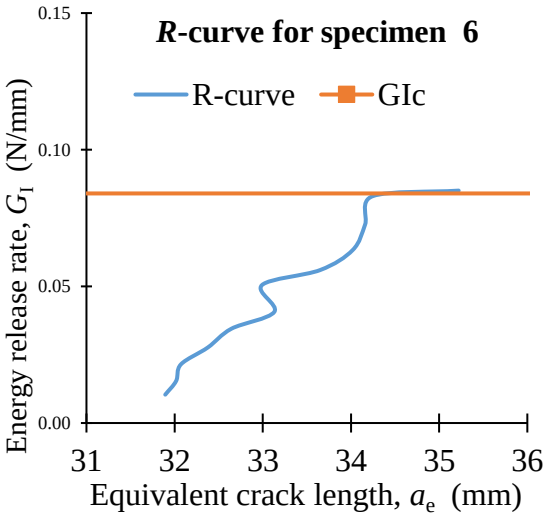

Figure 52 – *R*-curve for specimen 6

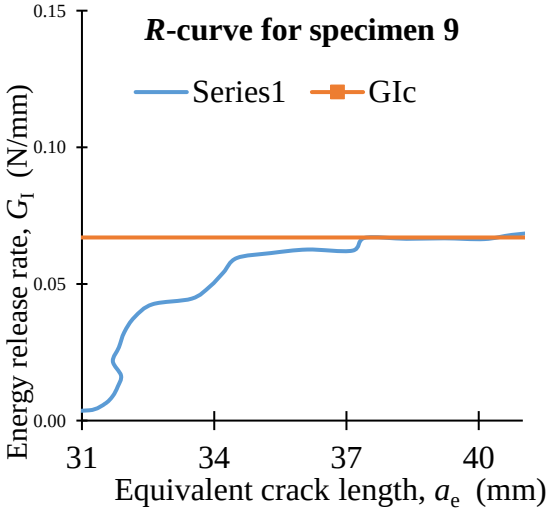

Figure 53 – *R*-curve for specimen 9

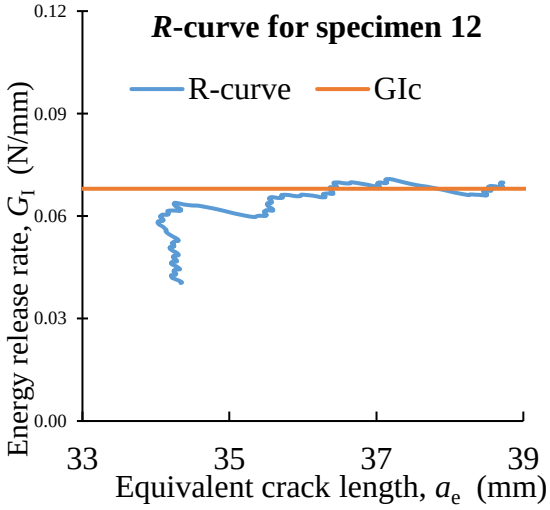

Figure 54 – *R*-curve for specimen 12

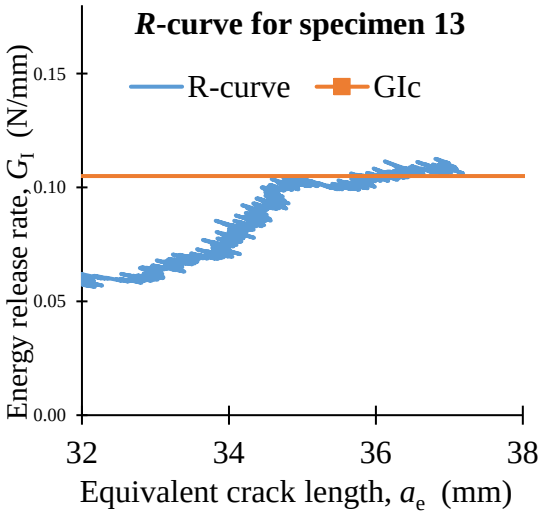

Figure 55 – *R*-curve for specimen 13

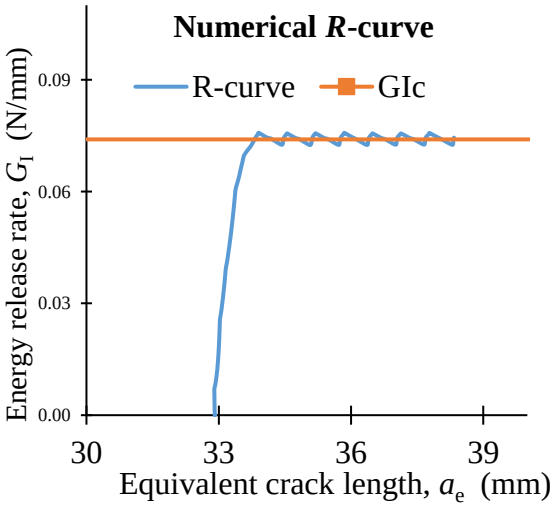

Figure 56 – *R*-curve for numerical simulation

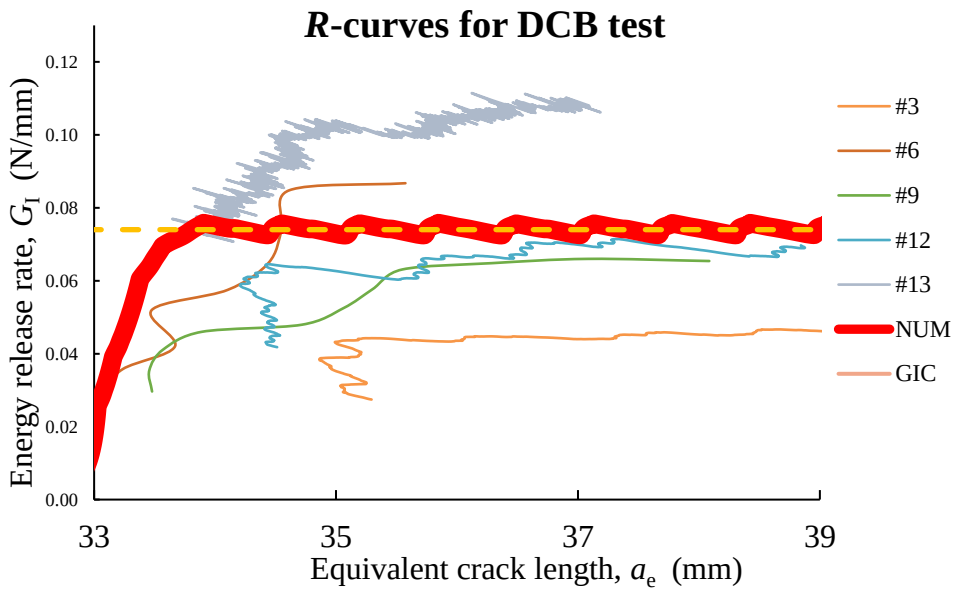

Figure 57 – *R*-curves for DCB test

The main advantage of this method is the fact that it is unnecessary to monitor the crack propagation during the test, being used instead an equivalent crack length obtained through the current compliance. Consequently, the fracture energy, G_{Ic}, is obtained exclusively from the *P*-*δ* curve. This method is known as the CBBM [64]. Table 8 presents a summary of the results obtained in the DCB test.

Table 8 – Summary of the results obtained in the DCB test

Specimen	P_{max} (N)	E_L (MPa)	I (mm^4)	G_{Ic} (N/mm)
3	9.870	7000	40.040	0.043
6	13.314	14300	28.351	0.086
9	14.980	4900	83.531	0.070
12	13.959	4000	86.519	0.065
13	12.793	7600	28.771	0.105
Average	12.983	7560	53.442	0.074
CoV	15%	54%	55%	32%

with P_{max} being to the maximum load and I to the second moment of area of the cross section, obtained through the equation (8).

$$I = \frac{Bh^3}{12} \tag{8}$$

The modulus of elasticity (E_L) shown in the Table 8 is more of an apparent modulus of elasticity, because the adhesive thickness was not taken into account when calculating it. This factor can justify the 54% variation between the modulus of elasticity values obtained.

3.3.2 ENF test

In total, eight ENF tests were performed. The first two specimens fractured in the central region of the span, as can be seen in Figure 58 and Figure 59 and, as such, it was not possible to obtain the G_{IIc} value from them. In the remaining ones, the crack propagation was noticeable and then the data obtained from these specimens were processed.

Figure 58 – Specimen 4 fractured after the ENF test

Figure 59 – Specimen 5 fractured after the ENF test

Figure 60 shows a specimen during an ENF test. In this image, it is possible to verify that the black lines marked on the specimen which are initially aligned, by this time of the test were no longer aligned. Moreover, in the left end of the specimen it is also possible to observe the lack of alignment of the arms. These aspects reflect the occurrence of shear loading at the crack's end.

Figure 60 – Loaded specimen in the ENF test

Figure 61 shows a specimen after the stress relief in the ENF test. In this specimen, before the test, the a_0 was at the first marked line and, in the image, it is possible to see a propagation beyond the fourth line.

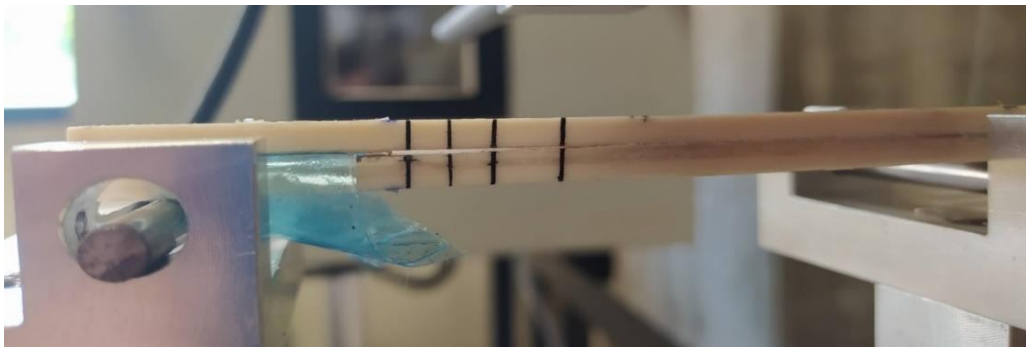

Figure 61 – Condition of a specimen after the ENF test

Similarly to what occurred for the DCB tests, the displacement and the corresponding applied load for each instant are extracted directly from the test program. The graph in Figure 62 presents the *P-δ* curves for all specimens tested with the ENF test directly after the extraction of the data from the machine with minimal processing. This figure also shows the numerical curve obtained.

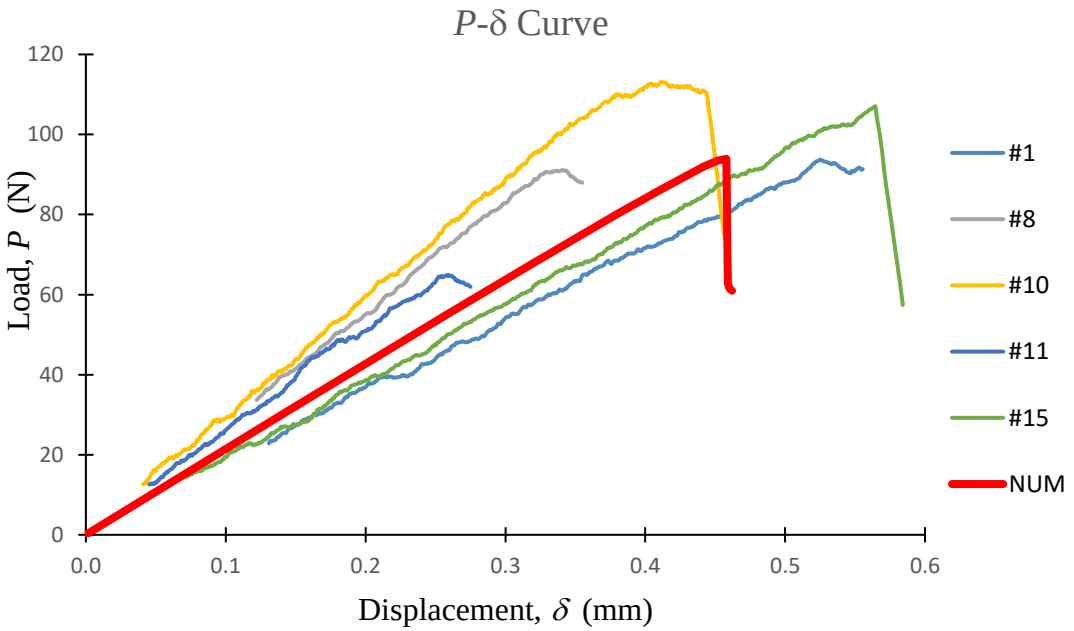

Figure 62 –*P-δ* curves of the ENF tests

Considering only the initial slope of the curve in Figure 62, it is possible to obtain the stiffness values (inverse of the compliance) for all the ENF specimens in Figure 63. The calculation of this slope is of particular importance, since it allows the correction of the displacement values obtained experimentally, and thus to reduce measurement errors.

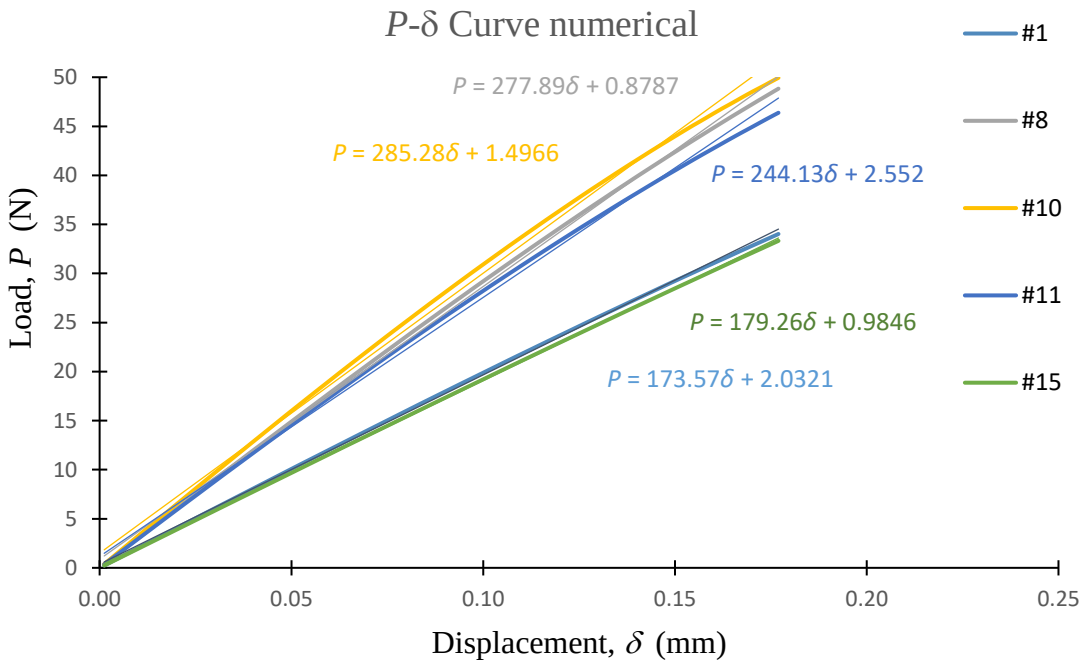

Figure 63 – Values for the specimens' stiffness in the ENF test

Following a similar strategy to the one used in the DCB tests, a data reduction scheme based on Timoshenko's beam theory and on the concept of equivalent crack was applied for the ENF tests (CBBM for ENF). Once again, this scheme was intended to overcome the difficulties associated with monitoring the crack length during the test, with the aggravating factor that in the ENF test it would be even more complicated to determine the crack length during the test, since the crack grows with the specimen arms in close contact. Therefore, the compliance in the ENF test can be obtained by equation (9) [64] using the Timoshenko beam theory,

$$C = \frac{3{a_e}^3 + 2L^3}{12E_L I} + \frac{3L}{10G_{LR}Bh} \tag{9}$$

This equation can be used to estimate the flexural modulus (E_f) considering the initial value of compliance (C_0) and crack length (a_0) yielding,

$$E_f = \frac{3{a_0}^3 + 2L^3}{12I}\left(C_0 - \frac{3L}{10G_{LR}Bh}\right)^{-1} \tag{10}$$

Equation (9) can also be employed to estimate the equivalent crack length (a_e) in the course of the test as a function of the current compliance (C), which leads to

$$a_e = \left[\left(\left(C - \frac{3L}{10G_{LR}Bh}\right)12E_f I - 2L^3\right)\frac{1}{3}\right]^{\frac{1}{3}} \tag{11}$$

Therefore, applying the Irwin-Kies equation (equation (6)) and the equivalent crack procedure, the pure mode II energy release rate is obtained by equation (12) [64].

$$G_{II} = \frac{9P^2 {a_e}^2}{16B^2 E_f h^3} \quad (12)$$

Following this procedure, the monitoring of the crack length during the test becomes unnecessary, which is very advantageous taking into account the inherent difficulty to follow the crack in the ENF test. In fact, in this fracture test, the crack propagates with their faces in close contact, which makes difficult the clear identification of its tip.

The obtained *R*-curves (G_{II} vs. a_e) are plotted in Figure 64 to Figure 69. As for Figure 70, it represents all the said curves in the same graph.

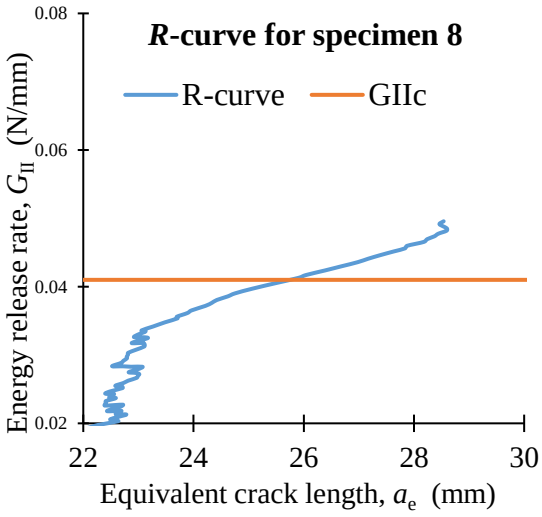

Figure 64 – *R*-curve for specimen 8

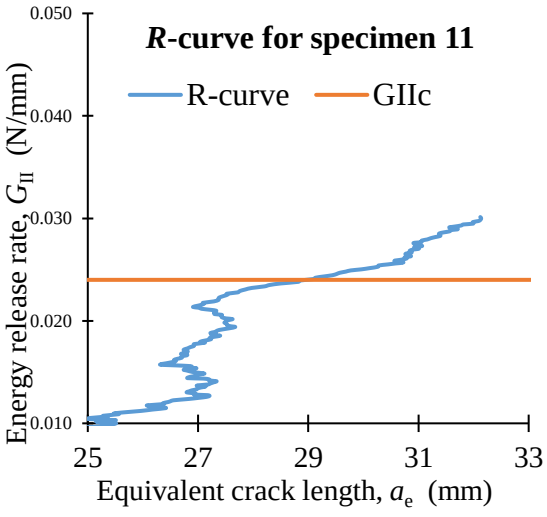

Figure 65 – *R*-curve for specimen 11

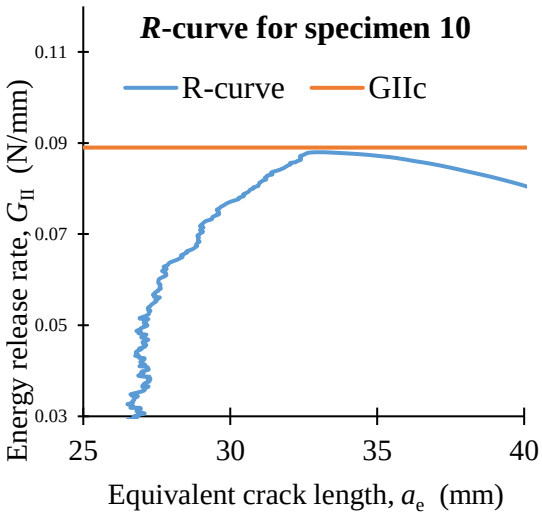

Figure 66 – *R*-curve for specimen 10

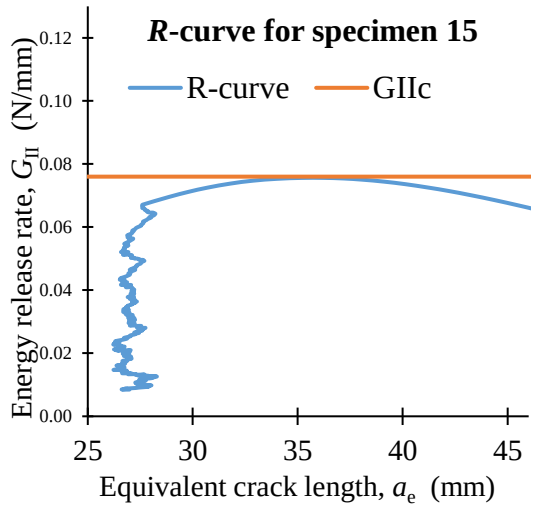

Figure 67 – *R*-curve for specimen 15

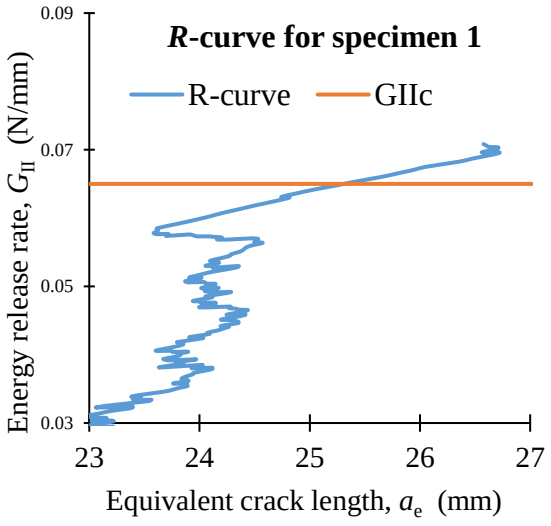

Figure 68 – *R*-curve for specimen 1

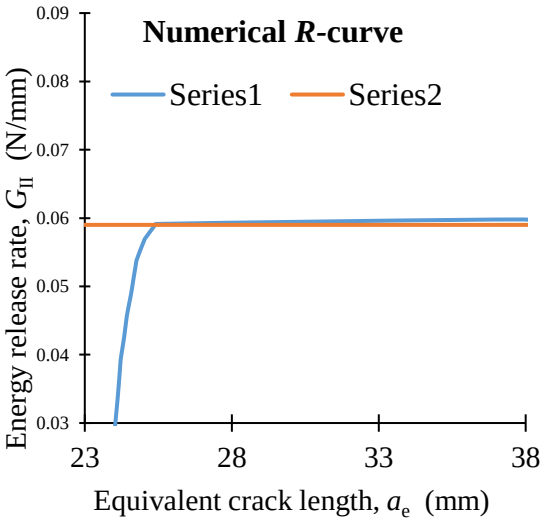

Figure 69 – Numerical *R*-curve

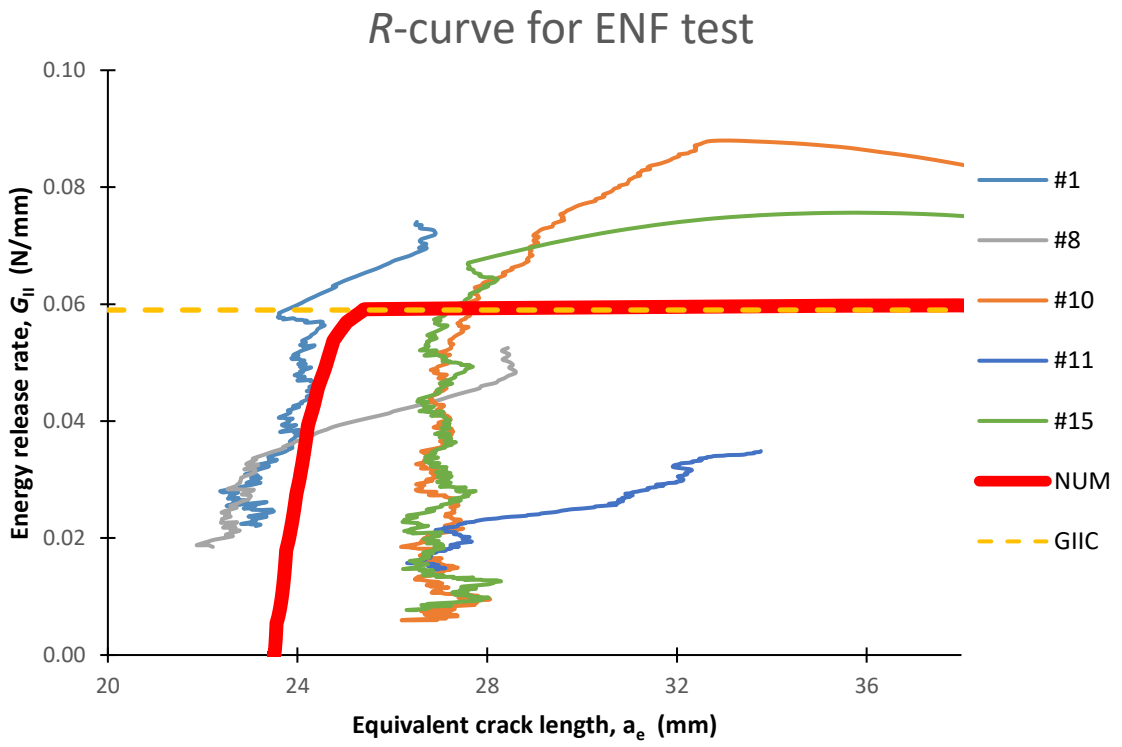

Figure 70 – *R*-curves for ENF test

Table 9 presents a summary of the results obtained in the ENF test.

Table 9 – Summary of the results obtained in the ENF test

Specimen	P_{max} (N)	E_f (MPa)	I (mm^4)	G_{IIc} (N/mm)
1	239.8	7735	54.0	0.065
8	219.8	10941	58.7	0.041
10	113.1	18349	41.6	0.089
11	103.6	12851	44.7	0.024
15	268.9	13106	47.9	0.076
Average	189.0	12597	49.4	0.059
CoV	40%	31%	14%	45%

3.4 Discussion of results

In this subchapter, the obtained results are discussed.

3.4.1 DCB test

In every *P-δ* curve (Figure 49), a gradual increase of the load in direct proportionality with the displacement is visible at the beginning, followed by a sharp decrease of the load value. This allows the conclusion that there was a crack propagation in all the specimens.

The obtained experimental *R*-curves were presented in Figure 51 to Figure 55. In all the curves, a plateau is presented, the region with almost zero slope (marked by the red trace). This region corresponds to the self-similar crack growth, which allows the measurement of an accurate value for the fracture energy G_{Ic}. On the other hand, Figure 56 presents the obtained numerical curve. In order to plot this curve, the mean dimensions (a_0, B and h) and the mean Young's modulus of every specimen of the experimental tests were considered. In addition, the numerical load-displacement and *R*-curve ensuing from the DCB test were included in Figure 49 and Figure 57, respectively. Despite the large scatter, typical of a natural material like bone, it can be concluded that both numerical curves represent well the overall trends observed experimentally. It is also important to highlight that the simulation routine is so well accomplished that the value obtained in the numerical *R*-curve is exactly the expected one (overlapped on the yellow dashed line in Figure 57).

In the literature, no articles characterising the bond between bone cement and the bone by means of a DCB test were found; however, Wang and his team [63] did this characterisation using the BCS test. As exemplified in Figure 71, this is a test in which a

material A (in the figure "bone") is bonded to a material B (in the figure "biomaterial") and the opposite surface of these materials is bonded to two accessories (in the figure "holder"). There is a pre-crack (in the figure "*a*") and a tensile force is applied at the end of the pre-crack on each accessory.

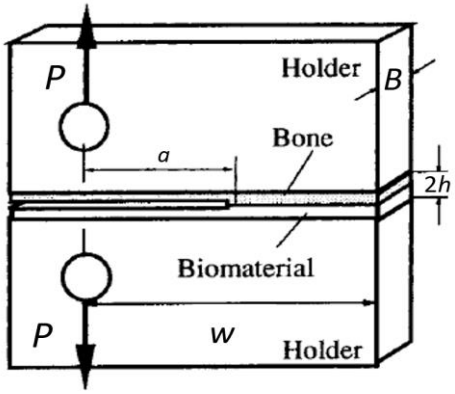

Figure 71 – Schematic representation of BCS specimen [63]

This test tends not to reveal the value of G_{Ic} very clearly, because the FPZ does not develop in a self-similar way. This happens since, as the specimen is very short, the compressive stresses that settle at the edge of the crack prematurely confine the FPZ. Nevertheless, if one looks only to the bone-cement region (bonded joint), the shape resembles a DCB, because the height of this region is much smaller than its length. Therefore, it is assumed that for bonded joints that length problem is somehow attenuated by the circumstance that the shape of the area of interest has a similar configuration to that of the DCB specimen. For these reasons, it was agreed that it is legitimate to compare the results obtained with the DCB test to those obtained by these authors. Accordingly, the G_{Ic} value obtained experimentally in this project was 0.074 N/mm, which is of the same order of the values obtained by Wang *et al* [63], i.e., between 0.038 and 0.052 N/mm.

3.4.2 ENF test

When the first ENF test was performed, the specimen fractured in the central region of the span, i.e., in the region where the loading displacement was being applied. This means that the specimen fractured by the arm and not by the connection, which indicates that the bone resistance was exceeded, but not that of the connection. This data was considered dubious, because during the handling of the specimens it had been possible to observe that the application of a force, even if slight, would cause the bone and the cement to detach. It was assumed that this could be happening because the bonding area was too large and, therefore, in the second tested specimen it was tried to reduce this area by means of applying a notch in the bonding region on each side. In spite of this, when the test was repeated the specimen fractured again in the exact same region. Taking this into consideration, it was decided to increase the distance between the test supports with the objective to diminish the stiffness, thus promoting a shear stress at the crack' end before the specimen arms' failure. After

increasing the distance between the test supports, good results were obtained, as seen in Figure 60 and Figure 61, where there was shear and crack propagation.

From the *P-δ* curve, the test for the sample 6 was discarded because the load value never decreased and, due to this factor, it cannot be concluded that there was a crack propagation. Thus, Figure 62 represents the *P-δ* curves of all the tests that were considered valid. This, similarly to what occurred for the DCB test, englobes all the curves, which reveal a gradual increase of the load in direct proportionality with the displacement at the beginning, followed by a sharp decrease of the load value.

The *R*-curves obtained with the ENF test are represented between Figure 64 and Figure 68. Similarly to what happened in the DCB test, every curve presents a plateau that corresponds to self-similar crack growth, which allows the measurement of an accurate value of the fracture energy G_{IIc}.

Specimens 10 (Figure 66) and 15 (Figure 67) have shown similar curves. These specimens registered a larger length, which leads to a greater extent for crack extension, before the compressive effects of the loading point exert its spurious influence. For this reason, these tests present a curve with a high increasing slope, after the plateau.

Specimens 8 (Figure 64) and 11 (Figure 65) also present very similar *R*-curves, characterised by a steady-state increase with a slight plateau region. Comparing these two curves with the two beforementioned, there are two main points to highlight. The first is that, after the plateau, the G_{IIc} value does not suffer a decrease, and the second one is that the plateau occurs in a much lower value of G_{IIc}. Specimen 1 (Figure 68), in spite of also presenting a steady-state increase plateau, presents a G_{IIC} value much closer to the one obtained in the specimens referred in the previous paragraph. One reason for this steady-states increase is possibly the fact that the 2*L* value is lower in these last specimens and, consequently, the crack does not present a prominent region to propagate and soon starts to be confined.

Another important characteristic, which leads to the suspicion that the specimen's ideal dimensions are of extreme importance in the test (not only the distance between supports), is observed with a comparison between the graphs of the *R*-curves of specimens 8 (Figure 64) and 10 (Figure 66), and their dimensions in Table 6. As it can be seen, although both have a distance between supports of 90 mm, the dimensions of the specimen 8 are much larger, both 2*h* and *B*, and the G_{IIc} value is much lower. The specimen 11 is the one that shows the lowest G_{IIc} value and also the highest *B* value.

The progressive damage analysis of the ENF test provided a numerical load-displacement and a *R*-curve that were compared with the corresponding experimental ones in Figure 62 and Figure 70. Once again, it can be concluded that the overall tendencies of the experimental curves are adequately captured by the numerical

approach. This statement confirms the validity of the followed approach regarding accurate fracture characterisation of this bone/cement connection.

CONCLUSIONS

4.1 CONCLUSIONS

4.2 PROPOSAL OF FUTURE WORKS

4 CONCLUSIONS AND PROPOSALS OF FUTURE WORKS

4.1 CONCLUSIONS

Due to the high number of bone fractures that occur every year, leading to a reduction in the patient's quality of life and high costs, both for the health system and for society in general, there is an immediate need to act in this sector and develop solutions to improve the quality of life for these patients. With this motto came the BoFraPla project, financed by FCT, which proposes to develop a new bone fracture fixation system. This dissertation is part of this project's activities, being its main goal to develop appropriate methodologies and procedures for fracture characterisation of bonded joints with cortical bone tissue and bone cement.

From a thorough literature review it was found that, although bone cement has been used for more than fifty years, there are few references to its mechanical characterisation, particularly regarding the characterisation of the fracture process between bone cement and cortical bone tissue. Thus, in this report, a characterisation of the bond between these two materials in pure mode I and pure mode II is proposed. For this characterisation, it is suggested the application of two tests widely used in the characterisation of bonded joints and already used in the characterisation of cortical bone tissue: the Double Cantilever Beam test (DCB) and the End-notched flexure test (ENF).

In the experimental component, multiple specimens made with bonded joints between cortical bone and bone cement were fabricated. From these specimens, some were used for DCB tests and others for ENF tests. From the tests, load-displacement curves were plotted and then resistance-curves (*R*-curves) as well, from which the value of the respective rates (G_{Ic} and G_{IIc}) were obtained. The results were treated through the Compliance Based Beam Method (CBBM), using the equivalent crack length, which became a great advantage and necessity, given the difficulty in monitoring the crack length during the tests.

In the numerical component, two types of simulations were performed. The first, addressed the Young's Modulus value for each specimen by an inverse process, due to the fact that bone is a natural and heterogeneous material. For the DCB case, with the actual dimensions of each specimen and with multiple iterations of numerical simulations in the Abaqus® software, the value of the initial numerical stiffness was adjusted, by changing the longitudinal elastic modulus, until it corresponded to the experimental stiffness. In the ENF tests, the initial values of compliance and crack

length were used to estimate an equivalent flexural modulus using the specimen compliance equation. The second type of simulation focused on the results validation obtained experimentally. With this aim, numerical simulations involving cohesive zone modelling were performed in order to mimic crack initiation and propagation in the DCB and ENF tests. In both cases, the numerical load-displacement and *R*-curves represent well the observed trends which proves the suitability of the proposed procedure concerning fracture characterisation of this bone/cement connection.

In this study, it was found that, in the DCB test, the difference in the specimen dimensions has no direct implication on the results obtained. On the other hand, in the ENF test these dimensions already have a direct repercussion on the performance of the specimen in the test. Therefore, in the ENF tests, the length of the specimens should be as long as possible, in order to have more space for the crack propagation before the emergence of the compressive effects induced by the loading cylinder, which prevents its propagation.

A value of 0.074 N/mm was obtained for the energy release rate in mode I (G_{Ic}) and 0.059 N/mm for G_{IIc} with a coefficient of variance of 32% and 45%, respectively. It can be concluded that these values are in agreement with ones published in the literature. Regardless, it should be noticed that these values of fracture energy can be visualised as somewhat low, which highlights the need to increase the research on this topic. In fact, it would be interesting that these bone cements could have higher toughness values, envisaging its application in the context of bone repair. Besides, it would also be relevant that they present a high stiffness, so that they may be used in a fixation system in which the aim is to have a rigid body.

4.2 PROPOSAL OF FUTURE WORKS

For a better characterisation under pure mode II, in the future it would be useful to perform more ENF tests that present a higher crack propagation region, i.e., using specimens with greater length (2*L*). With this factor, it is believed that the number of specimens that can originate valid tests will be higher, and the scatter obtained in this work will be reduced.

Since the work performed in the framework of this dissertation was only focused on fracture characterisation under pure modes (I and II), it is necessary to perform tests under mixed mode I+II, in order to obtain the fracture criterion representative of this connection.

Another suggestion for a future work would be to repeat the tests, but keeping the specimens hydrated. Since the human body has multiple body fluids, under real conditions the bones remain hydrated; however, it would be necessary to find a solution that simulates the body fluids in a correct way. Saline solution, as referred to

in some papers to keep bones hydrated, does not have exactly the same constitution as body fluids and when put together with bone cement causes its degradation.

In addition, an interesting aspect is the study of fracture under fatigue under pure and mixed-mode loading of this bone/cement connection. The determination of fatigue behaviour and lives as function of mode mixture may be regarded as a valid contribution to understand and improve the quality of bone repair.

REFERENCES AND OTHER SOURCES OF INFORMATION

5 REFERENCES AND OTHER SOURCES OF INFORMATION

[1] J. Ebnezar, *Textbook of Orthopedics: With Clinical Examination Methods in Orthopedics*. JP Medical Ltd, 2010.

[2] M. J. Sánchez-Fernández, H. Hammoudeh, R. P. Félix Lanao, M. van Erk, J. C. M. van Hest, and S. C. G. Leeuwenburgh, "Bone-adhesive materials: clinical requirements, mechanisms of action, and future perspective," *Adv. Mater. Interfaces*, vol. 6, no. 4, p. 1802021, 2019.

[3] A. Completo and F. Fonseca, *Fundamentos de Biomecânica Músculo-Esquelética e Ortopédica*. Publindústria, Produção de Comunicação, Lda, 2011.

[4] A. Remedios, "Bone and bone healing," *Vet. Clin. North Am. small Anim. Pract.*, vol. 29, no. 5, pp. 1029–1044, 1999.

[5] G. J. Tortora and B. H. Derrickson, *Principles of anatomy and physiology*. John Wiley & Sons, 2018.

[6] J. D. Heckman, R. W. Bucholz, and P. Tornetta III, *Rockwood and green's fractures in adults*, Eighth edi. LWW, 2015.

[7] J.-Y. Rho, L. Kuhn-Spearing, and P. Zioupos, "Mechanical properties and the hierarchical structure of bone," *Med. Eng. Phys.*, vol. 20, no. 2, pp. 92–102, 1998.

[8] "The skeletal system." http://what-when-how.com/nursing/the-musculoskeletal-system-structure-and-function-nursing-part-1/ (accessed May 11, 2021).

[9] R. W. Hertzberg, R. P. Vinci, and J. L. Hertzberg, *Deformation and fracture mechanics of engineering materials*, Fifth Edit. John Wiley & Sons, 2020.

[10] D. G. Steele and C. A. Bramblett, *The anatomy and biology of the human skeleton*. Texas A&M University Press, 1988.

[11] A. Mehra and J. Ebnezar, *Orthopedics Quick Review*. Jaypee Brothers,Medical Publishers Pvt. Limited, 2010.

[12] F. Libonati and L. Vergani, "Understanding the structure–property relationship in cortical bone to design a biomimetic composite," *Compos. Struct.*, vol. 139, pp. 188–198, 2016.

[13] A. Proença, *Ortopedia Traumatologia*, 2nd editio. Imprensa da Universidade de Coimbra, 2008.

[14] A. I. Caplan, "Mesenchymal stem cells: cell–based reconstructive therapy in orthopedics," *Tissue Eng.*, vol. 11, no. 7–8, pp. 1198–1211, 2005.

[15] H. Denny and S. Butterworth, *A guide to canine and feline orthopaedic surgery*. John Wiley & Sons, 2008.

[16] F. Judas, P. Palma, R. Falacho, and H. Figueiredo, "Estrutura E Dinâmica Do Tecido Ósseo," 2012.

[17] A. H. Burstein, J. M. Zika, K. G. Heiple, and L. Klein, "Contribution of collagen and mineral to the elastic-plastic properties of bone," *JBJS*, vol. 57, no. 7, pp. 956–961, 1975.

[18] M. Mehta *et al.*, "Influences of age and mechanical stability on volume, microstructure, and mineralization of the fracture callus during bone healing: Is osteoclast activity the key to age-related impaired healing?," *Bone*, vol. 47, no. 2, pp. 219–228, 2010, doi: https://doi.org/10.1016/j.bone.2010.05.029.

[19] X. Wang, X. Shen, X. Li, and C. M. Agrawal, "Age-related changes in the collagen network and toughness of bone," *Bone*, vol. 31, no. 1, pp. 1–7, 2002.

[20] R. Orozco, J. M. Sales, and M. Videla, *Atlas of internal fixation: fractures of long bones*. Springer Science & Business Media, 2013.

[21] "Greenstick fracture | Radiology Reference Article | Radiopaedia.org." https://radiopaedia.org/articles/greenstick-fracture (accessed Aug. 28, 2021).

[22] J. H. Breasted, "Edwin Smith surgical papyrus in facsimile and hieroglyphic transliteration with translation and commentary," *Chicago Univ. Chicago Orient. Inst. Publ.*, 1930.

[23] M. E. Müller, S. Nazarian, P. Koch, and J. Schatzker, *The comprehensive classification of fractures of long bones*. Springer Science & Business Media, 2012.

[24] B. D. Browner, *Traumatismos do sistema musculoesquelético: fraturas, luxações, lesões ligamentares*. Manole, 2000.

[25] M. S. Jones and B. Waterson, "Principles of management of long bone fractures and fracture healing," *Surg.*, vol. 38, no. 2, pp. 91–99, 2020.

[26] M. T. Reeder, B. H. Dick, J. K. Atkins, A. B. Pribis, and J. M. Martinez, "Stress fractures," *Sport. Med.*, vol. 22, no. 3, pp. 198–212, 1996.

[27] D. Taylor, "Observations on the role of fracture mechanics in biology and medicine," *Eng. Fract. Mech.*, vol. 187, pp. 422–430, 2018.

[28] H. L. Frost, "Presence of microscopic cracks in vivo in bone," *Henry Ford Hosp. Med. J.*, vol. 8, no. 1, pp. 25–35, 1960.

[29] R. Ben Kahla, A. Barkaoui, and T. Merzouki, "Age-related mechanical strength evolution of trabecular bone under fatigue damage for both genders: Fracture risk evaluation," *J. Mech. Behav. Biomed. Mater.*, vol. 84, pp. 64–73, 2018, doi: https://doi.org/10.1016/j.jmbbm.2018.05.006.

[30] J. B. Phelps, G. B. Hubbard, X. Wang, and C. M. Agrawal, "Microstructural heterogeneity and the fracture toughness of bone," *J. Biomed. Mater. Res.*, vol.

51, no. 4, pp. 735–741, 2000.

[31] F. J. O'Brien, D. Taylor, and T. C. Lee, "Microcrack accumulation at different intervals during fatigue testing of compact bone," *J. Biomech.*, vol. 36, no. 7, pp. 973–980, 2003, doi: https://doi.org/10.1016/S0021-9290(03)00066-6.

[32] F. J. O'Brien, D. Taylor, and T. Clive Lee, "The effect of bone microstructure on the initiation and growth of microcracks," *J. Orthop. Res.*, vol. 23, no. 2, pp. 475–480, 2005, doi: https://doi.org/10.1016/j.orthres.2004.08.005.

[33] M. R. M. Aliha, S. Bagherifard, S. Akhondi, S. S. Mousavi, A. Mousavi, and H. Parsania, "Fracture and microstructural study of bovine bone under mixed mode I/II loading," *Procedia Struct. Integr.*, vol. 13, pp. 1488–1493, 2018.

[34] E. F. McCarthy and F. J. Frassica, "The pathophysiology of fractures," in *Pathology of Bone and Joint Disorders: With Clinical and Radiographic Correlation*, 2nd ed., Cambridge: Cambridge University Press, 2014, pp. 101–113.

[35] N. K. Sharma, R. Pal, D. K. Sehgal, and R. K. Pandey, "Application of elastic-plastic fracture mechanics to determine the locational variation in fracture properties of cortical bone," *Mater. Perform. Charact.*, vol. 3, no. 3, pp. 429–447, 2014.

[36] F. Libonati and L. Vergani, "Bone toughness and crack propagation: an experimental study," *Procedia Eng.*, vol. 74, pp. 464–467, 2014.

[37] T. L. Norman, D. Vashishth, and D. B. Burr, "Fracture toughness of human bone under tension," *J. Biomech.*, vol. 28, no. 3, pp. 309–320, 1995.

[38] Q. D. Yang, B. N. Cox, R. K. Nalla, and R. O. Ritchie, "Re-evaluating the toughness of human cortical bone," *Bone*, vol. 38, no. 6, pp. 878–887, 2006.

[39] R. K. Nalla, J. H. Kinney, and R. O. Ritchie, "Mechanistic fracture criteria for the failure of human cortical bone," *Nat. Mater.*, vol. 2, no. 3, pp. 164–168, 2003.

[40] F. A. M. Pereira, J. J. L. Morais, N. Dourado, M. De Moura, and M. I. R. Dias, "Fracture characterization of bone under mode II loading using the end loaded split test," *J. Mech. Behav. Biomed. Mater.*, vol. 4, no. 8, pp. 1764–1773, 2011.

[41] C. L. Malik, S. M. Stover, R. B. Martin, and J. C. Gibeling, "Equine cortical bone exhibits rising R-curve fracture mechanics," *J. Biomech.*, vol. 36, no. 2, pp. 191–198, 2003.

[42] D. Vashishth, "Rising crack-growth-resistance behavior in cortical bone:: implications for toughness measurements," *J. Biomech.*, vol. 37, no. 6, pp. 943–946, 2004.

[43] R. K. Nalla, J. J. Kruzic, J. H. Kinney, and R. O. Ritchie, "Effect of aging on the toughness of human cortical bone: evaluation by R-curves," *Bone*, vol. 35, no. 6, pp. 1240–1246, 2004.

[44] J. J. L. Morais *et al.*, "The double cantilever beam test applied to mode I fracture characterization of cortical bone tissue," *J. Mech. Behav. Biomed. Mater.*, vol. 3, no. 6, pp. 446–453, 2010.

[45] R. O. Ritchie, M. J. Buehler, and P. Hansma, “Plasticity and toughness in bone,” 2009.

[46] M. F. de S. F. de Moura, A. M. B. de Morais, and A. G. de Magalhães, *Materiais compósitos: materiais, fabrico e comportamento mecânico*. 2010.

[47] L. F. M. da Silva, A. G. de Magalhaes, and M. F. S. F. de Moura, *Juntas adesivas estruturais*. Publindústria Portugal, 2007.

[48] R. D. S. G. Campilho, “Repair of composite and wood structures,” Faculty of Engineering of Porto University, 2009.

[49] E. G. Buettmann and M. J. Silva, “Development of an in vivo bone fatigue damage model using axial compression of the rabbit forelimb,” *J. Biomech.*, vol. 49, no. 14, pp. 3564–3569, 2016.

[50] A. A. Abdel-Wahab, A. R. Maligno, and V. V Silberschmidt, “Micro-scale modelling of bovine cortical bone fracture: Analysis of crack propagation and microstructure using X-FEM,” *Comput. Mater. Sci.*, vol. 52, no. 1, pp. 128–135, 2012.

[51] J. Yan, K. B. Clifton, J. J. Mecholsky Jr, and R. L. Reep, “Fracture toughness of manatee rib and bovine femur using a chevron-notched beam test,” *J. Biomech.*, vol. 39, no. 6, pp. 1066–1074, 2006.

[52] F. Judas, P. Palma, R. I. Falacho, and H. Figueiredo, “Estrutura e dinâmica do tecido ósseo,” 2012.

[53] W. Murphy, J. Black, and G. W. Hastings, *Handbook of biomaterial properties*. Springer, 2016.

[54] R. B. Ashman, S. C. Cowin, W. C. Van Buskirk, and J. C. Rice, “A continuous wave technique for the measurement of the elastic properties of cortical bone,” *J. Biomech.*, vol. 17, no. 5, pp. 349–361, 1984, doi: 10.1016/0021-9290(84)90029-0.

[55] C. H. Turner, T. Wang, and D. B. Burr, “Shear strength and fatigue properties of human cortical bone determined from pure shear tests.,” *Calcif. Tissue Int.*, vol. 69, no. 6, 2001.

[56] S. Li, A. Abdel-Wahab, and V. V Silberschmidt, “Analysis of fracture processes in cortical bone tissue,” *Eng. Fract. Mech.*, vol. 110, pp. 448–458, 2013.

[57] Y. H. An and R. A. Draughn, *Mechanical testing of bone and the bone-implant interface*. CRC press, 1999.

[58] K. J. Koester, J. W. Ager, and R. O. Ritchie, “The true toughness of human cortical bone measured with realistically short cracks,” *Nat. Mater.*, vol. 7, no. 8, pp. 672–677, 2008.

[59] T. Willett, D. Josey, R. X. Z. Lu, G. Minhas, and J. Montesano, “The micro-damage process zone during transverse cortical bone fracture: No ears at crack growth initiation,” *J. Mech. Behav. Biomed. Mater.*, vol. 74, pp. 371–382, 2017.

[60] F. A. M. Pereira, J. J. L. Morais, M. De Moura, N. Dourado, and M. I. R. Dias, “Evaluation of bone cohesive laws using an inverse method applied to the DCB test,” *Eng. Fract. Mech.*, vol. 96, pp. 724–736, 2012.

[61] M. De Moura, N. Dourado, J. J. L. Morais, and F. A. M. Pereira, “Numerical analysis of the ENF and ELS tests applied to mode II fracture characterization of cortical bone tissue,” *Fatigue Fract. Eng. Mater. Struct.*, vol. 34, no. 3, pp. 149–158, 2011.

[62] E. A. Zimmermann, M. E. Launey, H. D. Barth, and R. O. Ritchie, “Mixed-mode fracture of human cortical bone,” *Biomaterials*, vol. 30, no. 29, pp. 5877–5884, 2009.

[63] X. Wang and C. M. Agrawal, “Interfacial fracture toughness of tissue-biomaterial systems,” *J. Biomed. Mater. Res.*, vol. 38, no. 1, pp. 1–10, 1997.

[64] F. J. P. Chaves, L. F. M. Da Silva, M. De Moura, D. A. Dillard, and V. H. C. Esteves, “Fracture mechanics tests in adhesively bonded joints: a literature review,” *J. Adhes.*, vol. 90, no. 12, pp. 955–992, 2014.

[65] Elsevier, “ScienceDirect.” .

[66] NCBI, “Pubmed.” .

[67] N. Dourado, F. A. M. Pereira, M. De Moura, J. J. L. Morais, and M. I. R. Dias, “Bone fracture characterization using the end notched flexure test,” *Mater. Sci. Eng. C*, vol. 33, no. 1, pp. 405–410, 2013.

[68] F. G. A. Silva *et al.*, “Fracture characterization of human cortical bone under mode II loading using the end-notched flexure test,” *Med. Biol. Eng. Comput.*, vol. 55, no. 8, pp. 1249–1260, 2017.

[69] F. A. M. Pereira, M. de Moura, N. Dourado, J. J. L. Morais, J. Xavier, and M. I. R. Dias, “Determination of mode II cohesive law of bovine cortical bone using direct and inverse methods,” *Int. J. Mech. Sci.*, vol. 138, pp. 448–456, 2018.

[70] A. Vasilopoulos, G. Tsoucalas, V. Thomaidis, and A. Fiska, “Hans von Gersdorff and Hans Wechtlin; when battlefield surgery and anatomy met art,” *Int. Med.*, vol. 2, no. 1, p. 74, 2020, doi: 10.5455/im.68441.

[71] P. Hernigou, “Medieval orthopaedic history in Germany: Hieronymus Brunschwig and Hans von Gersdorff,” *Int. Orthop.*, vol. 39, no. 10, pp. 2081–2086, 2015.

[72] H.-L. Wang and L. Boyapati, “‘PASS’ principles for predictable bone regeneration,” *Implant Dent.*, vol. 15, no. 1, pp. 8–17, 2006.

[73] M. Chiapasco and M. Zaniboni, “Clinical outcomes of GBR procedures to correct peri-implant dehiscences and fenestrations: a systematic review,” *Clin. Oral Implants Res.*, vol. 20, pp. 113–123, 2009.

[74] W. Hofstetter and R. Egli, “Bone Repair and Fracture Healing,” 2014.

[75] A. J. Starr, “Fracture repair: successful advances, persistent problems, and the

psychological burden of trauma," *JBJS*, vol. 90, no. Supplement_1, pp. 132–137, 2008.

[76] C. Heiss and R. Schnettler, "Bioresorbierbare Knochenklebstoffe," *Unfallchirurg*, vol. 108, no. 5, pp. 348–355, 2005.

[77] K. J. Schreader, I. S. Bayer, D. J. Milner, E. Loth, and I. Jasiuk, "A polyurethane-based nanocomposite biocompatible bone adhesive," *J. Appl. Polym. Sci.*, vol. 127, no. 6, pp. 4974–4982, 2013.

[78] A. K. Gosain and P. S. E. F. D. Committee, "The current status of tissue glues: I. For bone fixation," *Plast. Reconstr. Surg.*, vol. 109, no. 7, pp. 2581–2583, 2002.

[79] Deutsche Institut für Normung e.V. (DIN), "DIN EN 923:2016-03: Adhesives - Terms and definitions," 2016. [Online]. Available: https://www.normadoc.com/english/din-en-923-2016-03-989282.html.

[80] K. O. Böker *et al.*, "Current State of Bone Adhesives—Necessities and Hurdles," *Materials (Basel).*, vol. 12, no. 23, p. 3975, 2019.

[81] P. Jordão, A. Bahute, U. Fontoura, and P. Marques, "Técnicas de cimentação femoral," *Rev. Port. Ortop. e Traumatol.*, vol. 21, no. 4, pp. 473–478, 2013.

[82] R. Vaishya, M. Chauhan, and A. Vaish, "Bone cement," *J. Clin. Orthop. trauma*, vol. 4, no. 4, pp. 157–163, 2013.

[83] S. Saha and S. Pal, "Mechanical properties of bone cement: a review," *J. Biomed. Mater. Res.*, vol. 18, no. 4, pp. 435–462, 1984.

[84] L. C. Chow, "Calcium Phosphate Cements," in *Monographs in Oral Science*, vol. 18, 2001, pp. 148–163.

[85] G. Dhatt, E. Lefrançois, and G. Touzot, *Finite element method*. John Wiley & Sons, 2012.

[86] A. Ural and S. Mischinski, "Multiscale modeling of bone fracture using cohesive finite elements," *Eng. Fract. Mech.*, vol. 103, pp. 141–152, 2013.

[87] B. N. Cox and Q. Yang, "Cohesive zone models of localization and fracture in bone," *Eng. Fract. Mech.*, vol. 74, no. 7, pp. 1079–1092, 2007.

[88] T. Siegmund, M. R. Allen, and D. B. Burr, "Modeling of bone failure by cohesive zone models," in *Mechanics Down Under*, Springer, 2013, pp. 217–230.

[89] É. Budyn and T. Hoc, "Multiple scale modeling for cortical bone fracture in tension using X-FEM," *Eur. J. Comput. Mech. Eur. Mécanique Numérique*, vol. 16, no. 2, pp. 213–236, 2007.

[90] S. Li, A. Abdel-Wahab, E. Demirci, and V. V Silberschmidt, "Fracture process in cortical bone: X-FEM analysis of microstructured models," in *Fracture Phenomena in Nature and Technology*, Springer, 2014, pp. 43–55.

[91] M. Wang, S. Li, A. vom Scheidt, M. Qwamizadeh, B. Busse, and V. V Silberschmidt, "Numerical study of crack initiation and growth in human cortical bone: Effect of micro-morphology," *Eng. Fract. Mech.*, vol. 232, p. 107051, 2020.

[92] D. F. Farrar, “Bone adhesives for trauma surgery: A review of challenges and developments,” *Int. J. Adhes. Adhes.*, vol. 33, pp. 89–97, 2012.

[93] DePuy Synthes, “DePuy CMW™ Heritage Bone Cements - Product Information,” 2016.

[94] Bahco, “Folhas de serrote manual - para metais. Nova SANDFLEX Bi-metal + Cobalto.” https://www.bahco.com/pt_pt/folhas-de-serrote-manual---para-metais--nova-sandflex-bi-metal---cobalto-pb_3906_.html (accessed Jun. 15, 2021).

[95] Sandvik, “R216.34-16050-AK32H 1620.” https://www.sandvik.coromant.com/pt-pt/products/pages/productdetails.aspx?c=r216.34-16050-ak32h 1620.

[96] Instron, “Máquina de ensaio de fadiga 8801.” https://www.directindustry.com/pt/prod/instron/product-18463-1662884.html.

[97] A. Ural and D. Vashishth, “Cohesive finite element modeling of age-related toughness loss in human cortical bone,” *J. Biomech.*, vol. 39, no. 16, pp. 2974–2982, 2006.

[98] M. De Moura, J. P. M. Gonçalves, A. T. Marques, and P. M. S. T. De Castro, “Modeling compression failure after low velocity impact on laminated composites using interface elements,” *J. Compos. Mater.*, vol. 31, no. 15, pp. 1462–1479, 1997.

[99] M. De Moura, J. J. L. Morais, and N. Dourado, “A new data reduction scheme for mode I wood fracture characterization using the double cantilever beam test,” *Eng. Fract. Mech.*, vol. 75, no. 13, pp. 3852–3865, 2008.

[100] M. De Moura, N. Dourado, and J. Morais, “Crack equivalent based method applied to wood fracture characterization using the single edge notched-three point bending test,” *Eng. Fract. Mech.*, vol. 77, no. 3, pp. 510–520, 2010.

[101] Simulia, “ABAQUS UNIFIED FEA.” https://www.3ds.com/products-services/simulia/products/abaqus/.